Higher-order near-field probes.

D10: Summary Report

Pivnenko, Sergey; Kim, Oleksiy S.; Nielsen, Jeppe Majlund; Breinbjerg, Olav

Publication date:
2012

Document Version
Publisher's PDF, also known as Version of record

Higher-Order Near-Field Probes

ESTEC Contract No. 22812/09/NL/JD/al

D10: Summary Report

S. Pivnenko, O. S. Kim, J. M. Nielsen, O. Breinbjerg

Department of Electrical Engineering, Electromagnetic Systems
Technical University of Denmark

July 2012

R757

Department of Electrical Engineering, Electromagnetic Systems
Technical University of Denmark
Ørsteds Plads, Building 348
DK-2800 Kgs. Lyngby, Denmark
Phone: +45 4525 3800, Fax: +45 4593 1634, Homepage: www.elektro.dtu.dk

CONTENTS

1. Introduction 3
1.1. Scope 3
1.2. Applicable documents 3
2. Comparison of Higher-Order Probe Correction Techniques 5
3. Implementation of the FFT/Matrix Inversion Technique 7
4. Measurement Procedure and Uncertainty Estimate 9
4.1. Update of the measurement procedure 9
4.2. Uncertainty budget 10
5. Design of Generic Wideband Near-Field Probe 13
5.1. Requirements to higher-order near-field probe 13
5.2. Selection of candidate antenna 14
5.3. Design of a scalable near-field probe 15
6. 1-3 GHz Prototype Probe: Manufacture and Test 18
6.1. Manufacture of 1-3 GHz probe prototype 18
6.2. S-parameters and radiation tests 19
6.3. Verification of antenna measurement procedure 21
6.4. Conclusions 25
7. 0.4-1.2 GHz Probe: Manufacture and Validation 26
7.1. Manufacture of the 0.4-1.2 GHz probe 26
7.2. S-parameters and radiation tests 27
7.3. 435 MHz first-order probe 29
7.4. Verification of antenna measurement procedure 31
7.5. Conclusions 34
8. Summary and Conclusions 35
References 37

1 Introduction

1.1 Scope

This is the final summary report of the work carried out in the project "Higher-Order Near-Field Probes" for the European Space Agency (ESA) under ESA contract no. 22812/09/NL/JD/al. The project is based on the Statement of Work [AD1] and DTU's proposal [AD2].

1.2 Applicable documents

[AD1] ESTEC Contract No. 22812/09/NL/JD/al, Appendix 1: Statement of Work.

[AD2] O. Breinbjerg, "Updated Proposal for Higher-Order Near-Field Probes. TEC-EEA/2008.385/LSD 2008.11.11 – ESA RFQ/3-12652/09/NL/ST". Report AR425, Technical University of Denmark, July 2009.

[AD3] O. Breinbjerg, T.B. Hansen, T. Laitinen, S. Pivnenko, J.M. Nielsen: Higher-order near-field probes. D1: Comparative Investigation of Higher-Order Probe Correction Techniques. Technical University of Denmark, Dept. of Electrical Engineering, May 2012. (IR 815)

[AD4] J.M. Nielsen and O. Breinbjerg: Higher-order near-field probes. D2: Spherical Near-Field Antenna Measurements with Higher-Order Probes at the DTU-ESA Facility. Volume 1: Implementation of the FFT/Matrix inversion technique. Technical University of Denmark, Dept. of Electrical Engineering, May 2012. (IR 816, 77p)

[AD5] T. Laitinen: Higher-order near-field probes. D2: Spherical Near-Field Antenna Measurements with Higher-Order Probes at the DTU-ESA Facility. Volume 2: Determination of Uncertainty Estimate by Simulations. Technical University of Denmark, Dept. of Electrical Engineering, April 2012. (IR 817, 44p)

[AD6] S. Pivnenko: Higher-order near-field probes. D2: Spherical Near-Field Antenna Measurements with Higher-Order Probes at the DTU-ESA Facility. Volume 3: Determination of Uncertainty Estimate by Measurements. Technical University of Denmark, Dept. of Electrical Engineering, May 2012. (IR 818, 16p)

[AD7] S. Pivnenko and J.M. Nielsen: Higher-order near-field probes. D2: Spherical Near-Field Antenna Measurements with Higher-Order Probes at the DTU-ESA Facility. Volume 4: Measurement Procedure. Technical University of Denmark, Dept. of Electrical Engineering, May 2012. (IR 819, 21p)

[AD8] S. Pivnenko, O.S. Kim, J.M. Nielsen, and O. Breinbjerg: Higher-order near-field probes. D3: Probe specifications. Technical University of Denmark, Dept. of Electrical Engineering, March 2012. (IR 820, 13p)

[AD9] S. Pivnenko, O.S. Kim, J.M. Nielsen, and O. Breinbjerg: Higher-order near-field probes. D4: Probe test plan and test procedure. Technical University of Denmark, Dept. of Electrical Engineering, March 2012. (IR 821, 8p)

[AD10] S. Pivnenko, O.S. Kim, J.M. Nielsen, and O. Breinbjerg: Higher-order near-field probes. D5: Probe design definition and justification. Technical

University of Denmark, Dept. of Electrical Engineering, March 2012. (IR 822, 21p)

[AD11] S. Pivnenko, O.S. Kim, J.M. Nielsen, and O. Breinbjerg: Higher-order near-field probes. D6: Probe manufacturing drawings. Technical University of Denmark, Dept. of Electrical Engineering, March 2012. (IR 823, 28p)

[AD12] S. Pivnenko, O.S. Kim, J.M. Nielsen, and O. Breinbjerg: Higher-order near-field probes. D7: Probe test report and design evaluation. Technical University of Denmark, Dept. of Electrical Engineering, March 2012. (IR 824, 26p)

[AD13] S. Pivnenko, O.S. Kim, J.M. Nielsen, and O. Breinbjerg: Higher-order near-field probes. D8: Updated test plan and test procedure. Technical University of Denmark, Dept. of Electrical Engineering, March 2012. (IR 825, 8p)

[AD14] S. Pivnenko, O.S. Kim, J.M. Nielsen, and O. Breinbjerg: Higher-order near-field probes. D9: P-band probe test report and evaluation. Technical University of Denmark, Dept. of Electrical Engineering, April 2012. (IR 826, 35p)

2 Comparison of Higher-Order Probe Correction Techniques

The purpose of WP1000 was to conduct a comparative investigation of higher-order probe correction techniques; i.e. techniques for retrieving the Q-coefficients of the spherical wave expansion of the antenna under test (AUT) that take into account the existence of the probe's azimuthal spherical modes with index μ different from ±1.

In recent years a number of such higher-order probe correction techniques have been reported. Since 2005 Laitinen, Pivnenko, and Breinbjerg have presented several correction techniques for special types of higher-order probes; these are the iterative technique [1]-[2], the odd-order technique [3]-[4] and the first-third order technique [5]-[6]. Laitinen et al. also developed the FFT/matrix-inversion for general higher-order probes; this was first reported in 2006 as an outcome of an ESA project [7] and later in [8]-[9]. In 2008-2009 Schmidt and Eibert reported a plane-wave technique that also allows general higher-order probes [10]-[11]. Hansen has recently reported a matrix technique [12] in conjunction with an earlier reported complex sources model of the probe [13]-[14] that also allows correction for general higher-order probes. All of these techniques [1]-[14] are aimed specifically at the probe correction in the near-field to far-field transformation. There exists another group of techniques that are more general in scope, since they aim at the correction of not only the properties of the probe, but several non-ideal mechanisms in the measurement; e.g. the scattering from the walls of the, possibly non-anechoic, measurement chamber; these are the test zone field (TZF) correction techniques by Black and Joy [15], Toivanen et al. [16], and Pogorzelski [17]-[18].

The comparative investigation has focused on the 3 entirely probe correction techniques that allow for general higher-order probes; these techniques are thus

- The FFT/matrix-inversion technique (by Laitinen, Pivnenko, Nielsen and Breinbjerg)
- The system matrix technique (by Hansen)
- The plane wave near-field-far-field technique (by Schmidt, Leibnitz and Eibert)

All 3 techniques allow for general higher-order probes with non-identical and non-symmetric ports – and for general AUTs.

The system matrix technique and the plane wave near-field-far-field technique allow for ϕ- as well as θ-scanning. The FFT/matrix-inversion technique allows for ϕ-scanning. In combination with the double-ϕ-step-θ-scanning the FFT/matrix-inversion technique allows also for θ-scanning; however with some experimentally observed limitations. The computational complexities are noticeable different. With N being the truncation number for the polar spherical modes, which is linearly related to the electrical size of the AUT minimum sphere, we have

- The FFT/matrix-inversion technique: $O(N^4)$
- The system matrix technique: $O(N^3)$
- The plane wave near-field-far-field technique: $O(N^2 \log N)$

However, this requires that the sampling densities are chosen to take full effect of the involved fast Fourier transforms (FFT) which may not always be practically desirable.

Furthermore, the computational complexity does not straightforwardly translate to the computational cost, i.e. the computation time, since this depends on several other factors like algorithm implementation, computer speed, and the actual truncation number which is typically in the range $10 < N < 350$.

The documented experimental tests of the 3 techniques are also noticeable different. The plane wave near-field-far-field technique has only been tested for $15 < N < 35$ with a centered AUT and a "weak" higher-order probe (i.e. the level of higher-order modes was rather low). The system matrix technique has been tested for $N = 120$ with an off-set AUT and a medium higher-order probe. The FFT/Matrix inversion technique has been tested for $75 < N < 210$ with an off-set AUT and strong higher-order probes. Furthermore, it has been tested extensively with respect to its sensitivity to random and systematic measurement errors (noise, drift, wall reflections, misalignment, channel balance calibration issues, etc.) over several years.

A direct experimental comparison between the FFT/matrix-inversion technique and the system matrix technique was reported in [19]. An off-set S-band AUT (with N slightly above 200) was first measured with a standard first-order probe to establish a reference solution and subsequently measured with a medium higher-order probe (0'th and 2'nd azimuthal modes at some –25 dB level, 3'rd azimuthal mode at some –17dB level, and all other azimuthal modes at maximum –43dB levels). This measured data from the higher-order probe was then processed with both the FFT/matrix-inversion technique and the system matrix technique. The measurements were conducted at the DTU-ESA Spherical Near-Field Antenna Test Facility. The differences between all 3 sets of results – for the opted 3dB part of the radiation pattern – were of the order of 0.05dB which was also the level of the 1σ measurement uncertainty. Hence these differences are not statistically significant and all 3 techniques thus yield radiation patterns of the same accuracy. However, the system-matrix technique data processing was noticeably faster (about 30s) than the FFT/matrix inversion technique (about 480s).

It is not possible at this stage to make any final conclusion as to whether one of these 3 higher-order probe correction techniques is generally advantageous in terms of region of validity, accuracy, computational cost, and ease of implementation. This would require a range of quantitative comparative investigations – involving as many measurements – beyond those conducted within the present study. The FFT/matrix-inversion technique is clearly the one that has been verified and tested most extensively – numerically and experimentally. Through numerous investigatory measurement projects it has become an operational higher-order probe correction technique at the DTU-ESA Spherical Near-Field Antenna Test Facility.

3 Implementation of the FFT/Matrix Inversion Technique

The implementation of the FFT/Matrix inversion technique deals with improvement of the existing higher-order probe correction software in terms of computation time and also adapting the existing software to the double ϕ-step θ-scanning scheme for higher-order probes.

The FFT/Matrix inversion technique was developed in the DOLFP project [7]. The implemented algorithm for the double ϕ-step θ-scanning data is based on the article [8]. This additional capability is integrated into the existing software for conventional ϕ-scanning.

The starting point of the algorithm is the transmission formula in terms of spherical waves, where the probe signal w of a dual polarized probe with ports p = 1,2 at the probe position described by the spherical coordinates r, θ, ϕ is written as follows:

$$w(r,\theta,\phi,\chi_p) = \frac{1}{2}\sum_{\substack{smn \\ \sigma\mu\nu}} Q_{smn} e^{im\phi} d^n_{\mu m}(\theta) e^{i\mu\chi_p} C^{sn(3)}_{\sigma\mu\nu}(kr) R^p_{\sigma\mu\nu} ,$$

where Q_{smn} are the spherical wave coefficients, describing the antenna under test (AUT), $d^n_{\mu m}(\theta)$ and $C^{sn(3)}_{\sigma\mu\nu}(kr)$ are the rotation and translation coefficients, respectively, and $R^p_{\sigma\mu\nu}$ are the probe response constants.

With conventional theta-scanning, the measurement sphere is covered with scanning in $\theta \in [0, 360° - \Delta\theta]$ and steps in $\phi \in [0, 180° - \Delta\phi]$. However, this approach cannot be used with the higher-order probes due to the asymmetry of the higher-order probe modes. Instead, the ϕ-step is doubled, such that ϕ covers $[0, 360° - 2\Delta\phi]$, while the θ-scan still covers the range $\theta \in [0, 360° - \Delta\theta]$. The measurement sphere is still covered with equidistant samples in both θ and ϕ. This is the double ϕ-step θ-scanning scheme which, after a rearrangement of the data, essentially is similar to the known ϕ-scanning scheme in the way the sphere is covered: The difference is that for the double ϕ-step θ-scanning, in the second half of the sphere, the probe is rotated 180° around the χ-axis, and scan and step axes are interchanged. For measurement points the distinction between scan and step axes is irrelevant and it is a matter of data organization. The scan and the subsequent rearranging in the double ϕ-step θ-scanning scheme is illustrated in Fig. 1. The probe χ-rotation of 180° comes into play in the transmission formula with the factor $e^{i\mu\chi}$. This factor becomes either +1 or −1, depending on μ and thus introduces the concept of even and odd coefficients of the Gm matrix [8]. For the details of the implementation of the data processing in the double ϕ-step θ-scanning scheme, see [AD4].

When performing antenna measurements with the double ϕ-step θ-scan, the number of sample points are $N'_\phi \times N'_\theta$. After rearranging the sampling points in θ and ϕ, the number of points are

$$N_\theta = \frac{N'_\theta}{2} + 1, \quad N_\phi = 2N'_\phi$$

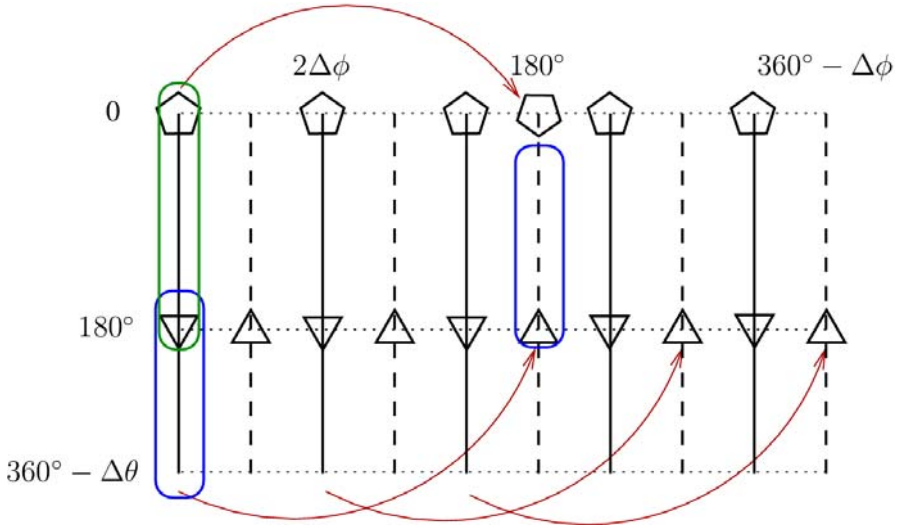

Fig. 1: Rearranging the theta-scans. Example shows grid with $N'_\phi = 5$, $2\Delta\phi = 72°$.

The possible double ϕ-step angles are shown in the Table 1 in section 4.1, which is sufficient for most common antenna measurements.

Several aspects have been dealt with to improve the computational speed of the FFT/matrix inversion technique. This includes a new computation scheme for the rotation coefficients, more efficient matrix pseudo-inverse implementation, and analysis of the executable program by profiling and subsequent in-line compilation of selected functions. A normalization of the transmission formula for preconditioning the system of equations was added, as suggested by Thorkild B. Hansen. This normalization improves on the condition numbers of the Gm matrices and enables the use of an iterative solver (conjugate gradient) instead of the matrix inversion. This, in turn, allows for a faster solution for the tested cases. Also, an outstanding issue with calculation of the channel balance has been clarified.

The FFT/Matrix Inversion technique with double ϕ-step θ-scanning capability was analyzed using both simulations and measurements. The simulations considered the following sources of inaccuracies: noise, channel balance uncertainty, and probe misalignment. The analyses were carried out using the forward transmission model for spherical waves; several different probe and antenna models were used. Additionally, studies on probe μ-mode truncation and on probe ν-mode truncation of a probe with zero field in the back-hemisphere were carried out. It was concluded that by utilizing truncation of some of the higher order μ-modes, the computation time can be reduced without introducing significant errors in the AUT pattern and directivity. This was analyzed for several different AUT and probe models. The ν-mode truncation of a probe with zero field in the back-hemisphere represents the case where a probe is used with a large absorber, blocking the radiation in the back hemisphere. Using such an absorber preserves the probe characteristics when it is first calibrated on one (antenna) tower and subsequently used on another (probe) tower with different support structures.

4 Measurement Procedure and Uncertainty Estimate

4.1 Update of the measurement procedure

The existing measurement procedure for first-order probe-corrected spherical near-field antenna measurements used at the DTU-ESA Facility was extended to accommodate the measurements with higher-order probes. The new elements in the measurement procedure are: calibration (measurement) of the higher order probe, measurement of the AUT with a higher-order probe using the ϕ-scanning technique or double ϕ-step θ-scanning technique and the corresponding steps of the data processing. The measurement procedure is documented in [AD7].

The updated measurement procedure consists of the following major steps:

1. Mechanical alignment of the antenna tower and the probe tower.
2. Flip-tests for correction of pointing and intersection.
3. Probe calibration.
4. Spherical near-field measurement of the AUT.
5. Spherical near-field measurement of the Standard Gain Horn (SGH) for AUT gain determination.
6. Measurement of input reflection coefficient of the AUT and the SGH.
7. Processing and plotting.

It is noted that in step 2, the probe (antenna on the probe tower) must satisfy the condition that its pattern is symmetric in the main planes. This condition is usually satisfied, when a Standard Gain Horn is used for probe calibration after the mechanical alignment. However, when the flip-test is done for an AUT on the antenna tower and a higher-order probe on the probe tower, the situation is different. If the higher-order probe has a symmetric pattern, the flip-test can be done and its results are valid. But, if the higher-order probe has a non-symmetric pattern in the angular sector towards the AUT, the flip-test should not be made with this probe. In this case, it is recommended to pre-align the tower in the required position (e.g. translation along roll axis) with a symmetric antenna on the probe tower.

In step 3, the calibration of the higher-order probe (HOP) consists of two parts: full-sphere measurements for each of the probe ports with a polarization-calibrated auxiliary antenna (AUX) and a channel balance measurement of the higher-order probe. Similar to the first-order probe calibration, a three-antenna polarization calibration is carried out, but in this case for the polarization calibration of the AUX. For convenience of manipulations of the antennas, the HOP pattern measurement is performed first, while the polarization calibration is performed next. The complete HOP calibration consists of the following measurements:

1. HOP port x is connected: full-sphere measurement for two AUX orientations (horizontal and vertical).
2. HOP port y is connected: full-sphere measurement for two AUX orientations.
3. SGH2 is mounted on the antenna tower, AUX is oriented horizontally: polarization scan 1.

4. HOP is mounted on the probe tower, SGH2 remains on the antenna tower: polarization scan 2.
5. HOP remains on the probe tower, AUX is mounted on the antenna tower and aligned for polarization: polarization scan 3.

For the details of the data processing related to the probe calibration, see [AD7].

In step 4, the measurement of the AUT can be done using a higher-order probe with the choice of either traditional ϕ-scanning scheme or the new double ϕ-step θ-scanning scheme. The spherical mode coefficients truncation indices and angular sampling intervals are determined as usual from the electrical dimensions of the AUT and its location with respect to the origin of the measurement coordinate system [20]. In the case of double ϕ-step θ-scanning scheme, the angular sampling grid should satisfy certain conditions: possible values of $\Delta\phi$ with resulting numbers, N_ϕ, and values, $2\Delta\phi$, of double ϕ-steps, and traditional number of steps, N'_ϕ, are shown in Table 1 [AD7]:

Table 1: List of possible double ϕ-steps

N_φ	$2\Delta\phi$ [°]	N'_φ	$\Delta\phi$ [°]
3	120	6	60
5	72	10	36
9	40	18	20
15	24	30	12
25	14.4	50	7.2
45	8	90	4
75	4.8	150	2.4
125	2.88	250	1.44
225	1.6	450	0.8

For the details of the data processing related to the AUT measurements, see [AD7].

4.2 Uncertainty budget

An uncertainty budget of the Spherical Near-Field (SNF) technique, similar to other near-field techniques, consists of some 25 terms. The number of terms taken into account and also their names may differ depending on the technique itself and its particular implementation, e.g. the kind of mechanical scanner. However, common features can be identified allowing definition of a common structure of the uncertainty budget, which then should be detailed for any particular implementation.

The common structure of the uncertainty budget of the SNF technique (also, generally, any antenna measurement technique) contains the following categories of uncertainty sources, according to their origin. The structure of the uncertainty budget presented below is applicable for relative pattern or directivity.

Category	Description
Mechanical	Related to the mechanical system, e.g. axes intersection and pointing, scan-plane planarity, probe position and orientation, etc.
Electrical	Amplitude and phase drift and noise, non-linearity, drift, cross-talk, amplitude and phase change in rotary joints, etc.
Probe-related	Probe pattern, probe polarization, channel balance
Stray signals	Multiple reflections, wall reflections, tower scattering
Acquisition	Scan-area truncation, systematic sampling point offset, etc.
Processing	Accuracy of the method itself, interpolation, aliasing, mode truncation, etc.

For the SNF technique implemented at the DTU-ESA Facility, the detailed uncertainty budget for the radiation pattern is presented in [AD6].

Compared to the use of the first-order probes, there are few changes in the uncertainty budget when using the higher-order probes.

One difference in the use of HOP as compared to the use of first-order probes is in the applied calibration procedures: for the HOP no separate polarization calibration is carried out since this is included into full-sphere measurement of the HOP pattern with a polarization-calibrated auxiliary antenna. Thus the uncertainty terms related to probe polarization are removed from the budget.

Another difference in the use of the HOP is that also a truncation limit on its μ-mode spectrum should be specified during the near-to-far-field transformation, in addition to the usual ν-mode truncation. A usual rule should be followed that the truncated normalized modes should preferably be below some −50 dB level in which case this truncation introduces negligible error into the probe pattern and thus into the calculated AUT pattern. In some cases, e.g. due to the use of a large absorber abruptly truncating the field in the back hemisphere or due to asymmetries and reflections in the probe and support structures, the mode spectra are decaying very slowly and truncation may be made at higher levels, e.g. at −30…−40 dB. In this case, probe pattern is represented with a certain error and it should be checked, if this in turn affects the AUT pattern, by performing several transformations including different number of probe modes and comparing the AUT patterns.

The higher-order probe developed in this project is based on so-called open-boundary ridged horn, which works on the principle of traveling wave antenna. One distinctive feature of this horn is that it does not have side walls and thus the electromagnetic field is not limited to the aperture as in traditional pyramidal or conical horns, but present everywhere around the ridges. As a result, it must be considered that the entire probe structure is carrying radiating currents and this must be taken into account in the design of the support structure and application of absorbers to cover the latter. The experiments with the prototype 1-3 GHz probe carried out within this project have shown that placement of the probe close to the absorbers (< 1 wavelength) significantly affects its radiation pattern and thus may result in improper probe correction, if the absorber layout on the probe tower is different from the antenna tower.

Proper placement of this (kind of) probe is such that it should be located far away from any support structure and any absorbers covering the latter. Proper distance is considered to be at least half-wavelength from the absorber tips, while the absorbers should preferably be longer than one wavelength. As this is difficult to ensure at 400 MHz, where the wavelength is 75 cm, any good "approximation" to these conditions should be considered as a goal.

The present location of the 0.4-1.2 GHz probe on the probe tower is illustrated in Fig. 2.

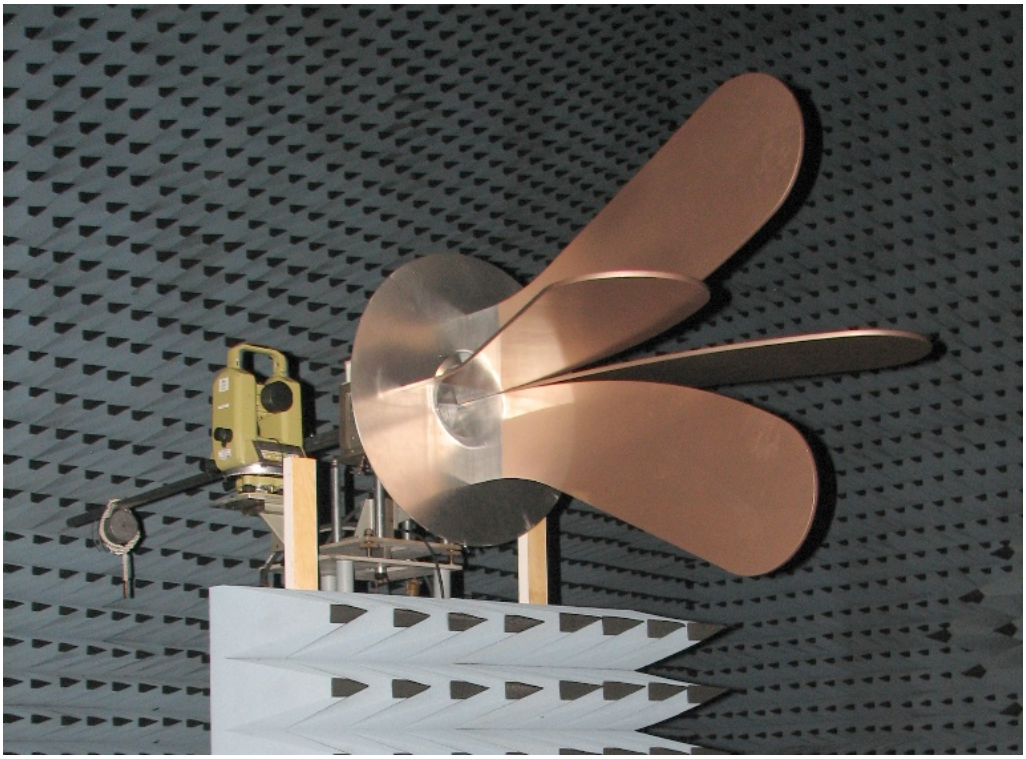

Fig. 2. The 0.4-1.2 GHz probe on the probe tower.

Proper location of the 0.4-1.2 GHz probe on the probe tower, i.e. when the probe is moved forward by some 40 cm to be well above and in front of the absorbers, requires modification of the probe tower table. The new probe tower table should be able to carry large weight of the probe assembly (probe + frame + counterweight ≈ 30 kg) while also providing location of the mounting frame at some 40 cm forward from the present location, i.e. above the present absorbers. A capability of axial translation of the table by some 20-40 cm is also very desirable for performing measurements with different distances between the AUT and probe for compensation of multiple reflections.

5 Design of Generic Wideband Near-Field Probe

5.1 Requirements to higher-order near-field probe

The characteristics of near-field probes and their analysis with application to spherical near-field antenna measurements were described in details in [AD8].

The requirements to the designed high-order near-field probe are summarized in the Table 2 below.

Characteristic	Requirement/description	Priority
1. Bandwidth	1:3 ratio; valid for pattern and scattering parameters	High
2. Radiation pattern	1) Pattern variation within $\theta = \pm 30°$: < 10 dB.	High
	2) Pattern level within $\theta = \pm[50° \ldots 76°]$ relative to the pattern peak: < –10 dB.	High
	3) Front-to-back ratio: > 10 dB	High
	4) Pattern symmetry: desirable in both planes	Medium
	5) Peak directivity: D ≈ [10…14] dBi (guideline)*	Medium
3. Ports orthogonality	Nominally orthogonal. Desirable axial ratio > 35 dB	High
4. Port-to-port isolation	High, < –35 dB.	High
5. Return loss	Low, < –10 dB	High
6. Radiation efficiency	Preferably high, > 0.8 (–1 dB)	Medium
7. Channel balance	Preferably close to (1,0)	Low
8. Size	Preferably small	Medium
9. Weight	Preferably low, < 8 kg	Medium
10. Scalability	Required by SOW	High
11. Manufacturing complexity	Preferably low	Medium
12. Stability	Must be mechanically and electrically stable	High
13. Cost	Preferably low	Low

* The value for the peak directivity is considered as guideline, since this was calculated using an approximate model of a rectangular horn, which is not necessarily used in the final design of the probe.

5.2 Selection of candidate antenna

Various antennas were considered and analyzed with respect to their suitability to the design goals [AD8]. After a preliminary review of their typical characteristics, several candidate antennas were chosen for a detailed consideration. For each type of antenna, a summary of its typical characteristics based on the published results is given in Table 3.

Table 3: Summary of the characteristics of the considered candidate antennas

Characteristic	Dual-polarized ridged horn	Dual-pol. inverted ridge horn	Open-boundary ridge horn	2×2 array of Bunny Ear Element (BEE)	Dual-pol. Log-Periodic Tooth (LPT)	2×2 array of Log-Periodic Dipoles (LPD)
Bandwidth	Up to 1:18	1:4	Up to 1:15	1:3 or more	Up to 1:18	1:3
Directivity	5-15 dBi ?	6-17 dBi	5-15 dBi	5-9(+3) dBi ? within 1:3 BW	9 dBi ?	8(+3) dBi
Front-to-back	10-25 dB	25-30 dB	5-25 dB	3-10 dB	< 9 dB ?	~ 20 dB
Pat. symm.	Yes ?	Yes (H-pl)	Yes ?	No ?	Almost	Almost
Cross-pol.	–25 dB ?	< –40 dB	< –35 dB	–25 dB ?	?	< –35 dB ?
Port-to-port	–25 dB ?	< –50 dB	< –35 dB	?	?	?
Return loss	< –10 dB	< –10 dB	< –10 dB	< –10 dB	< –10 dB	< –10 dB
Loss	~ 0.1 dB	~ 0.5 dB	~ 0.1 dB	0.1…1 dB	0.1…1 dB	0.1…1 dB
Size, (wavelength)	0.4×0.4×0.6 ?	0.7×0.7×2.1	0.7×0.7×0.6	0.7×0.7×1	0.6×0.6×1	0.6×0.6×1
Weight	2.4 kg ?	5 kg	1.2 kg	< 2 kg ?	< 2 kg ?	< 2 kg ?
Scalability	Good	Good	Good	Good/Poor	Good/Poor	Good/Poor
Complexity mechanical	High	High	High	Moderate	Moderate	Moderate
Complexity manual	Low	Low	Low	Low	Moderate	High
Complexity feed network	Low	High	Low	Moderate	Moderate	Moderate
Stability	High	High	High	High	Moderate	Moderate

Comparison of the characteristics of the potential candidate antennas allowed to exclude some of the antennas, since their characteristics are clearly worse compared to the other antennas.

Summarizing the analysis made in [AD8], initially, it was concluded that the most suitable candidate antenna would be the ridged horn, whereas the open-boundary ridge horn was ruled out due to relatively high front-to-back ratio reported in the literature. Further numerical study has shown that this ratio could be significantly improved by using an extended ground plane. Thus, the open-boundary ridge horn has been finally selected to be a generic antenna kind for the wide-band near-field probe.

5.3 Design of a scalable near-field probe

An open-boundary quad-ridged horn can be considered as a variation of a Vivaldi antenna, and therefore, it is inherently wide-band.

The generic design is sketched in Fig. 3. The antenna is composed of four orthogonal ridges extended from a cylindrical excitation cavity. The ridges open out exponentially from the mouth and terminate with a circular profile; the outer profile of the ridges is linear. The ridges are excited at the mouth (Fig. 4) by a coaxial line penetrating one ridge with its inner conductor extended and attached to an opposite ridge. An orthogonal excitation is displaced along z-axis. An exponential taper in the excitation cavity enhances the mechanical stability as well as facilitates the wideband matching of the antenna (Fig. 4). An extended circular ground plane ensures an improved front-to-back ratio. Simulations show that at the lower end of the operating frequency band, the suppression of the backlobes is improved by at least 5 dB.

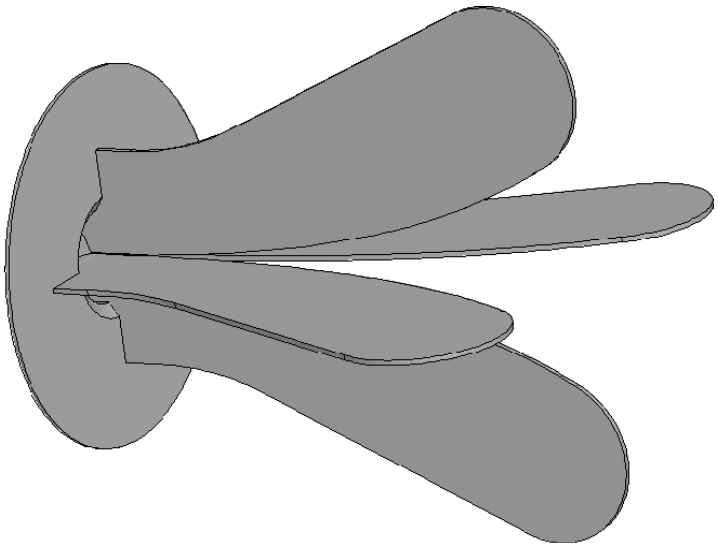

Fig. 3: Generic design of an open-boundary quad-ridged horn.

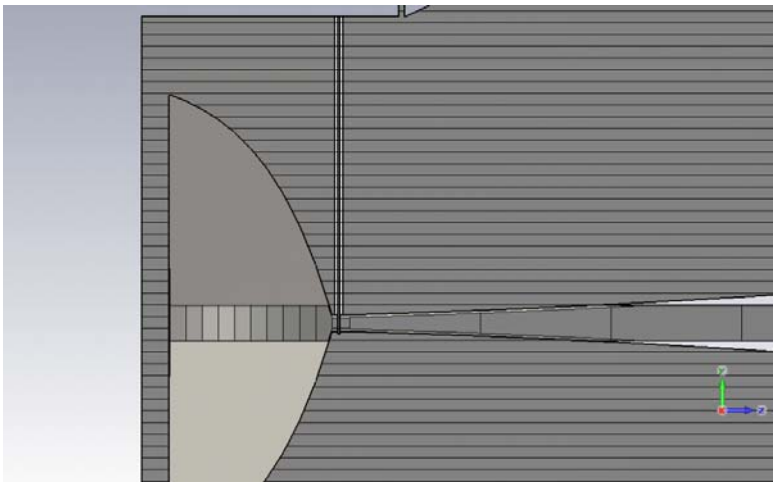

Fig. 4: Excitation of ridges by a coaxial line.

Although the ridged horn is inherently wide-band, its radiation properties can vary significantly with frequency, especially in the lower part of the working band. Therefore, a thorough optimization has been performed to achieve a design meeting all the stringent requirements in the 1:3 frequency band. The results are summarized in Table 4. The green colour marks satisfied requirements; the orange marks requirements that are satisfied in a part of the frequency band, but the obtained characteristics are deemed acceptable.

Table 4: Electrical requirements. Green: satisfied, orange: acceptable.

Characteristic	Requirement/description	Priority
1. Bandwidth	1:3 ratio; valid for pattern and scattering parameters	High
2. Radiation pattern	1) Pattern variation within $\theta = \pm 30°$: < 10 dB.	High
	2) Pattern level within $\theta = \pm[50°\ldots76°]$ relative to the pattern peak: < –10 dB.	High
	3) Front-to-back ratio: > 10 dB	High
	4) Pattern symmetry: desirable in both planes	Medium
	5) Peak directivity: D ≈ [10…14] dBi (guideline)*	Medium
3. Ports orthogonality	Nominally orthogonal. Desirable axial ratio > 35 dB	High
4. Port-to-port isolation	High, < –35 dB.	High
5. Return loss	Low, < –10 dB	High

The reflection coefficient is below –10 dB in the entire frequency band, as required (Fig. 5). The cross-coupling (port-to-port isolation) is below –50 dB. The radiation patterns at the lowest f_0 and the highest frequency $3f_0$ of the 1:3 band are shown in Fig. 6.

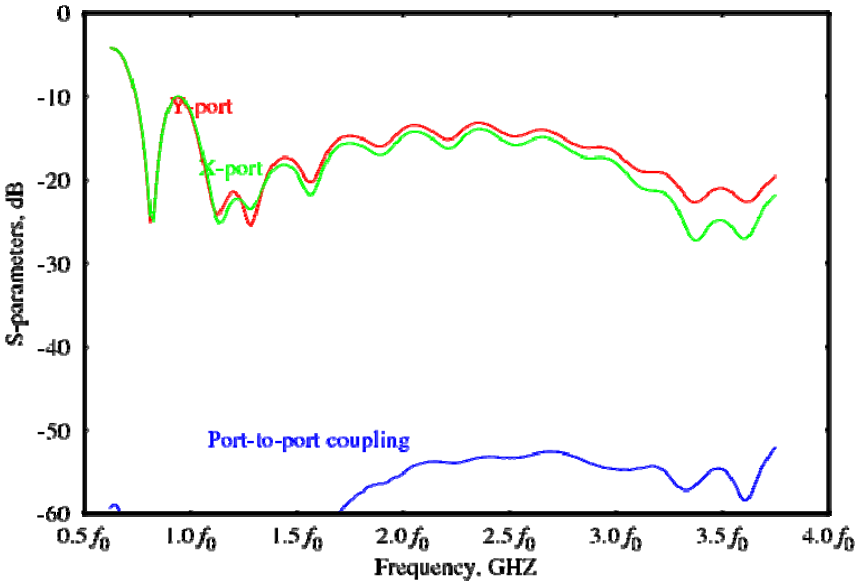

Fig. 5: The reflection coefficient and the cross-coupling.

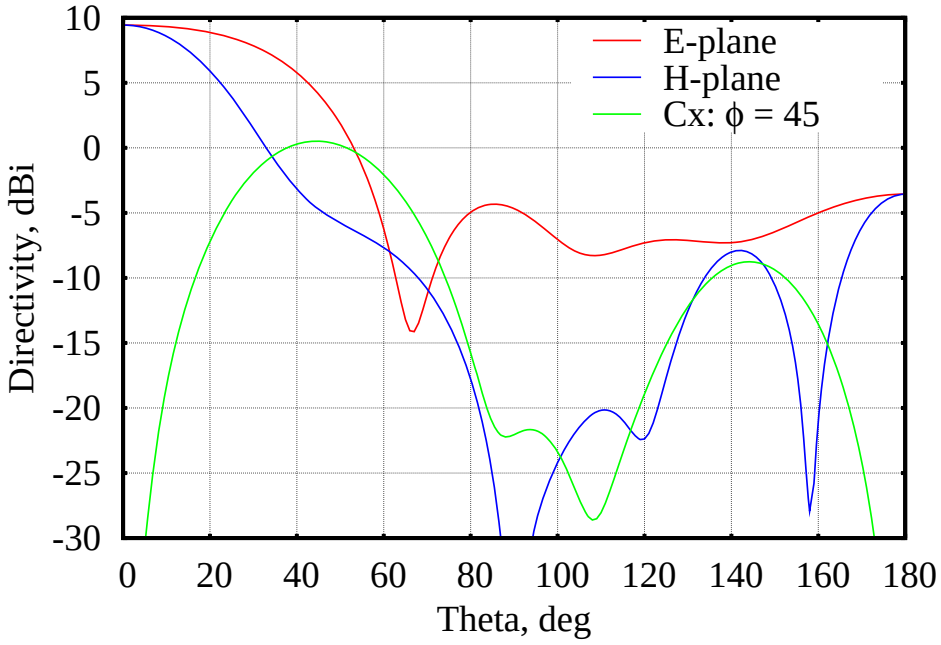

(a)

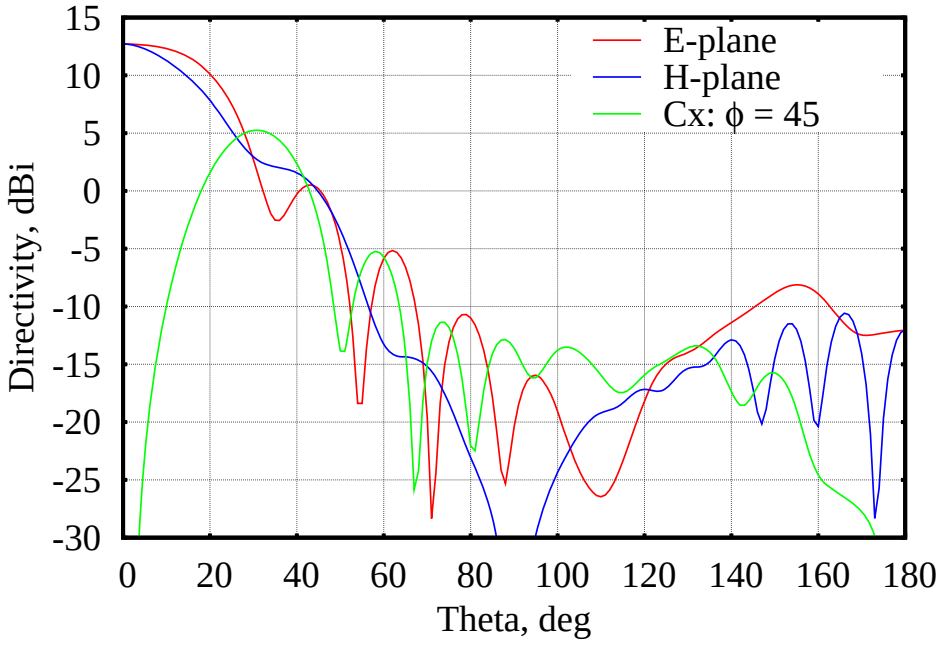

(b)

Fig. 6: Radiation pattern at the lowest f_0 (a) and the highest frequency $3f_0$ (b) of the 1:3 band.

6 1-3 GHz Prototype Probe: Manufacture and Test

6.1 Manufacture of the 1-3 GHz probe prototype

The 1-3 GHz probe prototype was manufactured at the mechanical workshop at the Department of Electrical Engineering at DTU during October-November 2010. The manufactured 1-3 GHz probe has the dimensions (W×H×L): 500×500×550 mm^3 and weight of 3.5 kg. The probe is shown in Fig. 7 attached to the mounting frame during pattern measurements.

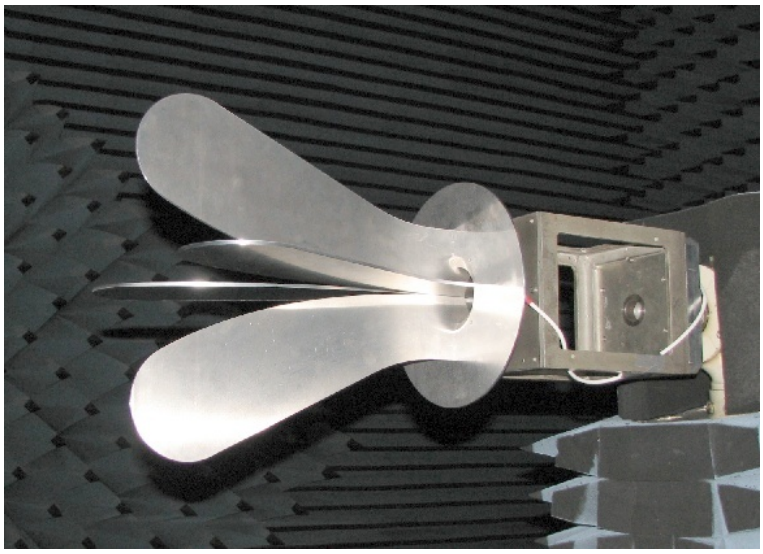

Fig. 7. Manufactured 1-3 GHz probe prototype during pattern measurements.

As noted in Section 5.3, the antenna is excited by two orthogonal pins located next to the ridge mouth (Fig. 4) and displaced along z-axis. Each pin is in fact the inner conductor of a coaxial cable penetrating a ridge; the dielectric of the coaxial cable terminates at that ridge, whereas its inner conductor extending across the gap between the ridges is fixed at the opposite ridge by a screw.

The standard EZ 141 50-ohm semi-rigid cable is utilized. Its inner conductor is 0.91 mm in diameter, and the insulation dielectric diameter is 2.98 mm.

When the generic design is scaled for the frequency band 1-3 GHz, the width of the ridges becomes 4 mm; and since the cable is not scalable, it appears that the width of the chamfered part of the ridges is less than the cable diameter. Consequently, the coax cable opening cut a part of the chamfer surface (Fig. 8a). This has a minor effect on the antenna input impedance and reflection coefficient, however, the port-to-port coupling increases due to excitation of asymmetric modes in the cavity. The latter are suppressed by introducing a symmetric notch in the opposite ridge, as shown in Fig. 8b. The dielectric insulation of the coaxial cable is terminated before it enters the chamfered surface (Fig. 8b).

At 1-3 GHz, the weight does not present any problem, and thus no special weight reduction technique was applied. The ridges were cut out of a 4-mm aluminum sheet and assembled with the cavity, which was machined from an aluminum bar.

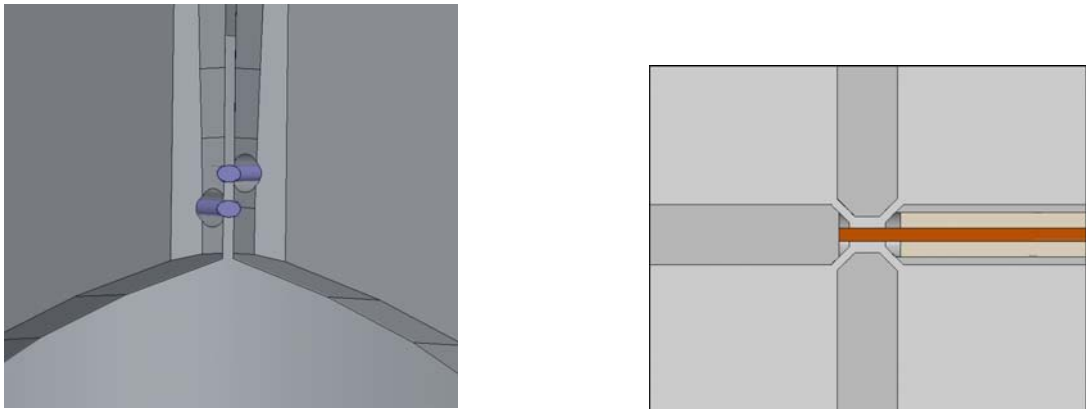

a b

Fig. 8: Excitation of the 1-3 GHz probe.

6.2 S-parameters and radiation tests

Measurement of the S-parameters was carried out in anechoic environment with a calibrated HP8753D vector network analyzer in the frequency band 0.7-4.7 GHz at 401 points. The results are shown in Fig. 9.

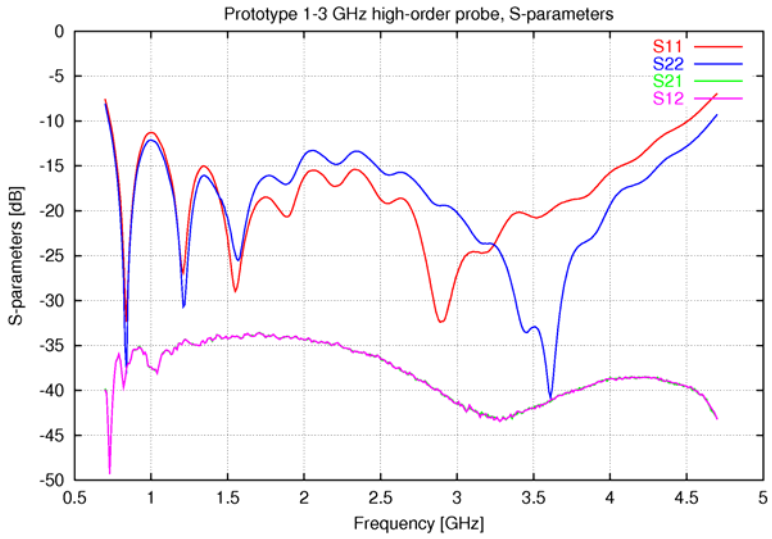

Fig. 9. Measured S-parameters of the 1-3 GHz probe prototype.

It is seen from Fig. 9 that the S11 and S22 parameters are within the requirements in the band from 0.75-4.50 GHz, while the S21 and S12 parameters are generally below the required −35 dB, but slightly above in the band 1.2-2.2 GHz with the maximum of −33.6 dB. This is noticeably higher than predicted by simulations (at least −50 dB). The reason for this behavior was investigated and it was found that there is slight mechanical deviation of the ridges around the feed point, which results in slight asymmetry, and thus the increased cross-coupling. According to conclusion from the mechanical workshop, the observed deviation was most probably caused by the stress in the rolled aluminum, the ridges were cut out of. Taking this effect into the consideration, it was decided to use cast aluminum plates for manufacturing of the 0.4-1.2 GHz probe.

The full-sphere radiation pattern of the 1-3 GHz probe was measured with the calibrated probe SP800 in the band 0.7-4.7 GHz with the step of 0.1 GHz.

The measured results are in good agreement with the predictions, as illustrated in Fig. 10, where the measured and simulated directivity are compared.

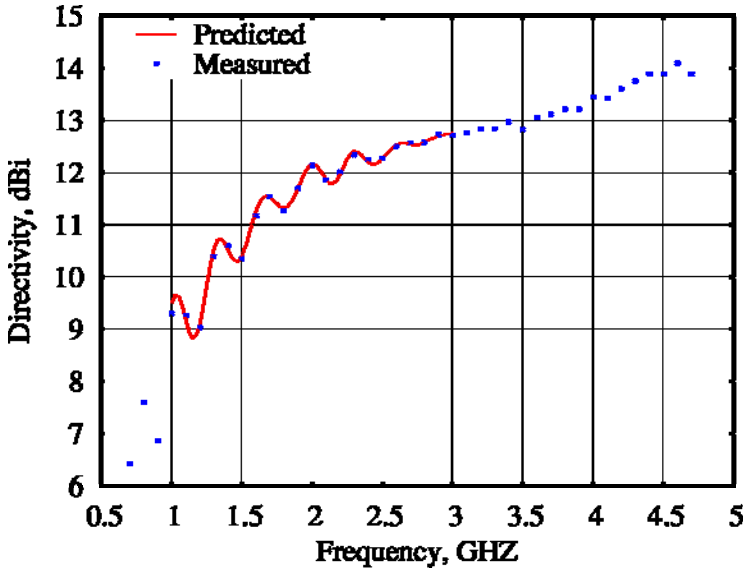

Fig. 10. Measured and simulated directivity of the manufactured 1-3 GHz probe.

The measured radiation pattern (Fig. 11) was analyzed for conformance to the requirements described in sub-section 5.1 [AD8]. It was found that most of the pattern requirements are satisfied, in particular, requirement 2.1: pattern variation within $\theta = \pm 30°$ is < 10 dB at all frequencies, and requirement 2.3: front-to-back ratio is > 10 dB at all frequencies. The requirement 2.2: normalized pattern level within $\theta = \pm[50°\ldots76°]$ to be < –10 dB is satisfied above 2 GHz, while between 1.1-1.9 GHz the maximum value of the normalized pattern level varies between –10…–8 dB with the highest value of –7.2 dB at 1.0 GHz.

Although, the antenna is well matched down to 750 MHz, the abrupt drop in the directivity renders it unusable as a probe below 1 GHz. On the other hand, it can be used with some precautions to as high as 4.5 GHz. The main lobe becomes very narrow at 3 GHz and above. Consequently, the variation within the AUT maximum field of view (±30°) becomes larger than the required 10 dB. However, if an AUT does not occupy the entire sphere of radius 3 m, its field of view is also narrower implying that the probe pattern variation remains within the required limit.

The requirement 3: ports orthogonality, desirable polarization axial ratio > 35 dB, is completely satisfied at all frequencies within 1-3 GHz, the observed axial ratio values are typically larger than 45 dB.

The radiation efficiency is within 0…–0.3 dB through the frequency range 1-3 GHz, thus the requirement 6 is also satisfied.

From the measured full-sphere radiation pattern, the spherical mode spectra were calculated and analyzed (Fig. 12). As expected, the 1-3 GHz probe clearly represents a high-order probe with significant amount of power in the modes with $\mu \neq \pm 1$.

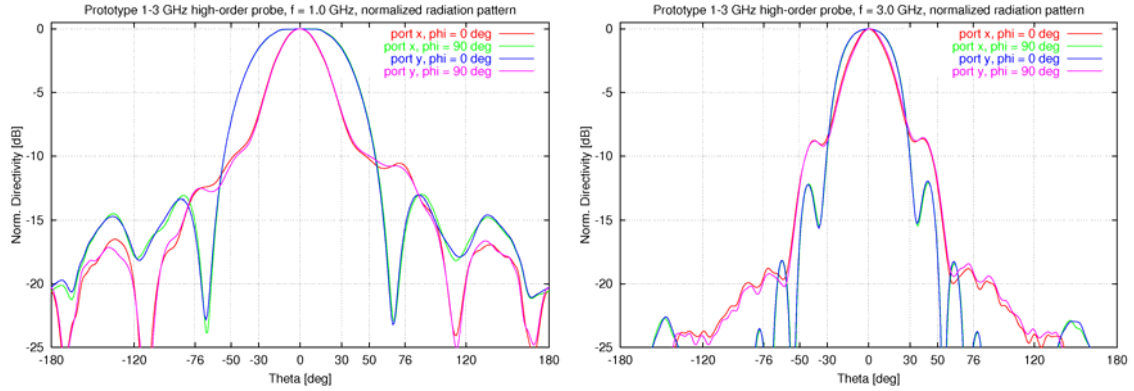

Fig. 11: Measured radiation pattern of the manufactured 1-3 GHz probe.

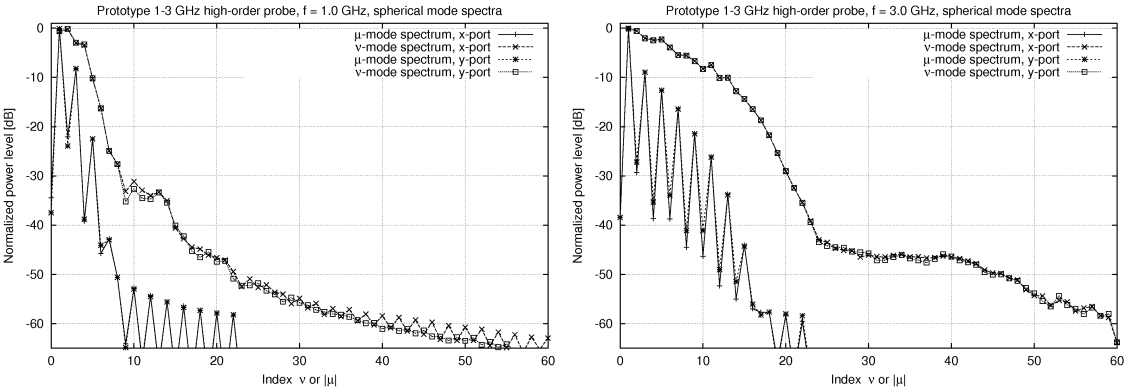

Fig. 12: Spherical mode spectra of the 1-3 GHz probe.

6.3 Verification of antenna measurement procedure

The detailed description of antenna measurement procedure verification with the 1-3 GHz prototype probe is given in [AD12]. Only few representative results are included here.

The antenna under test (AUT) is defined to be an offset-mounted SH800 horn. The offset results in significant increase of the minimum sphere for the AUT and thus the number of significant spherical modes in the spectrum. In addition, since the source of radiation is located close to the edge of the sphere, the significance of the probe pattern correction increases, for example, as compared to a uniformly excited aperture antenna of the same size. Therefore, an offset-mounted antenna represents probably the most difficult test case and obtaining good results for such antenna ensures also similarly good or better results for any other antenna of the same electrical size. The AUT used in the measurements is shown in Fig. 13.

The reference measurements of the AUT were carried out with high-quality dual-polarized first-order probes (FOP): with choked open-ended circular waveguide PRB15 at 1.4 GHz and 1.5 GHz and with a conical horn S2 at 2.9 GHz and 3.0 GHz.

Calibration of the 1-3 GHz high-order probe was carried out according to the updated measurement procedure; see section 4.1 and [AD7].

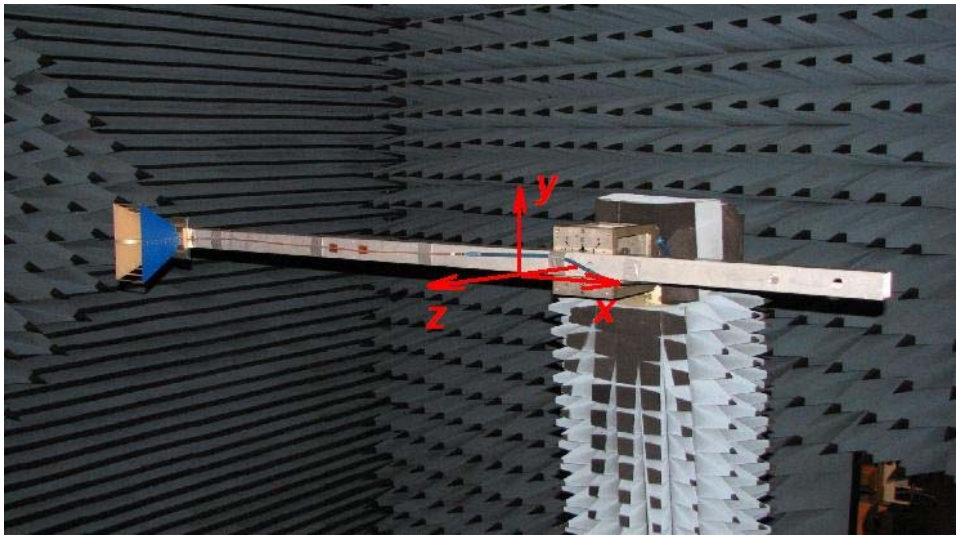

Fig. 13. Offset-mounted SH800 horn used as test object and the measurement coordinate system.

The measurement of the AUT was carried out two times: the measurement referred to hereafter as test 1 was carried out using the ϕ-scanning scheme, while the measurement referred to hereafter as test 2 was carried out using the double ϕ-step θ-scanning scheme.

Comparison of the results from the reference and test measurements has shown that the co-polar patterns agree well, while the level of the cross-polar pattern is noticeably higher for the data obtained with the high-order probe correction. An example of the far-field pattern comparison from test 1 versus reference is shown in Fig. 14. Similar results were obtained at other frequencies and thus not shown here.

Careful analysis of the data and the measurement setup has indicated that possible explanation for the increased cross-polar level might be the effect of the probe tower on the pattern of the high-order probe. The probe is an open structure and it is placed on the probe tower such that the surrounding absorbers are located very close to it and may thus change the pattern as compared to the pattern available from the calibration. Pictures of the probe placed in the usual position on the probe tower are shown in Fig. 15.

In order to reduce the effect of the surrounding absorbers the probe was attached to the probe frame through posts of different length, while performing a polarization scan for a linearly polarized horn SH800 as an AUT and observing the changes in the measured signal on the probe ports. It was found that it was necessary to move the probe forward by as much as 400 mm in order to obtain the expected symmetric polarization pattern. Pictures of the probe attached to the probe frame through 400 mm posts are shown in Fig. 16.

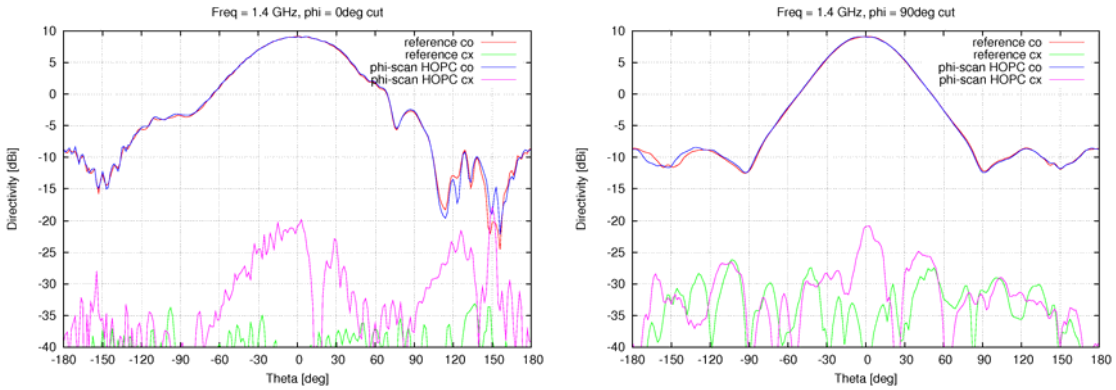

Fig. 14. Far-field pattern comparison from test 1 versus reference at 1.4 GHz (initial test).

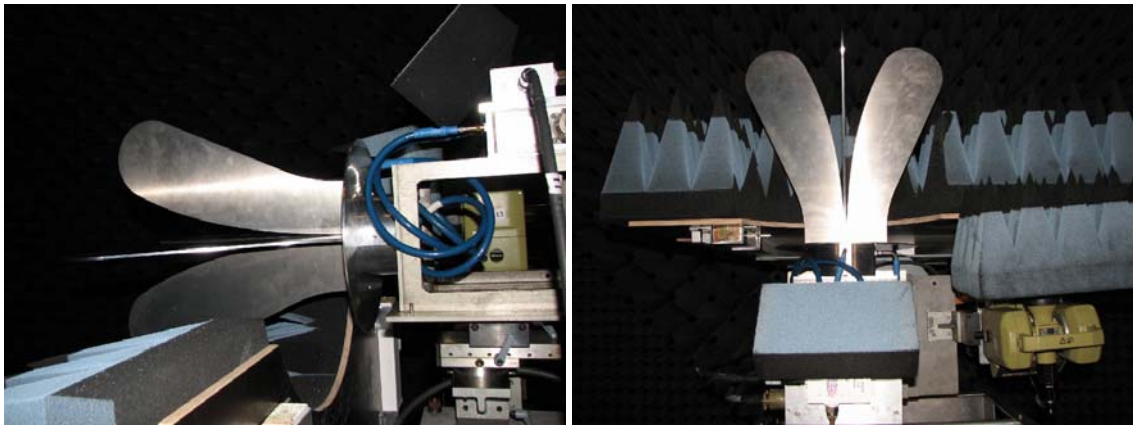

Fig. 15. High-order 1-3 GHz probe placed in the usual position on the probe tower: side view (left) and top view (right).

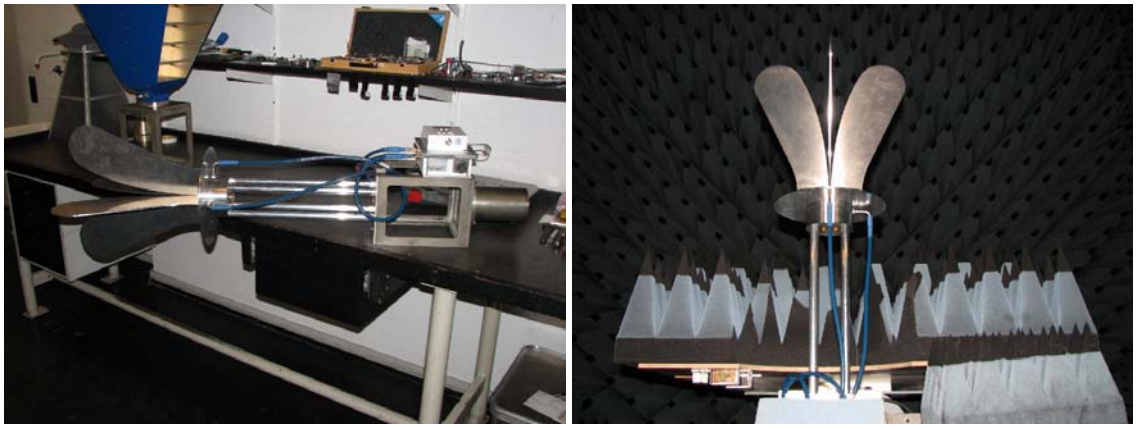

Fig. 16. High-order 1-3 GHz probe attached to the probe frame through 400 mm posts: side view (left) and probe on the probe tower, top view (right).

With the probe located in front of the absorbers on the probe tower, the test 1 and test 2 measurements of the AUT were repeated. It is noted that only these measurements were repeated, in view of the limited available time.

The obtained AUT far-field pattern from repeated test 1 and test 2 were then compared to the reference AUT far-field pattern. The examples of the far-field pattern comparison from repeated test 1 versus reference are shown in Fig. 17 at 1.4 GHz and from repeated test 2 versus reference are shown in Fig. 18 at 2.9 GHz.

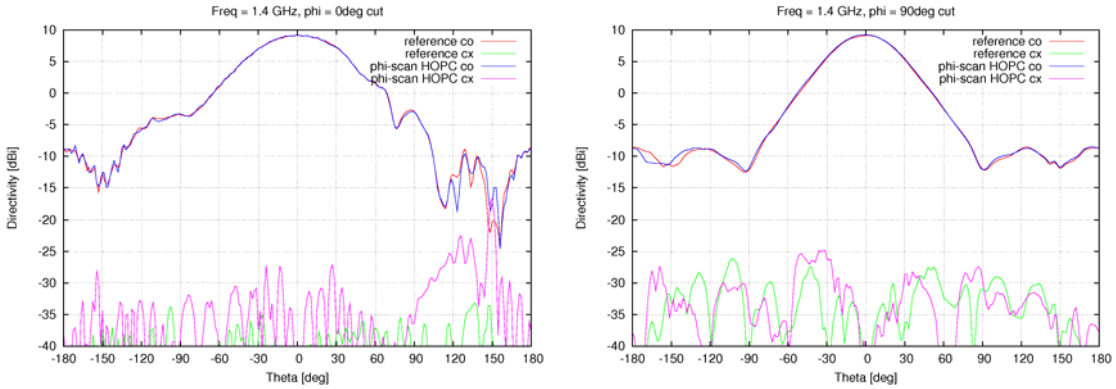

Fig. 17. Far-field pattern comparison from test 1 versus reference at 1.4 GHz (repeated test).

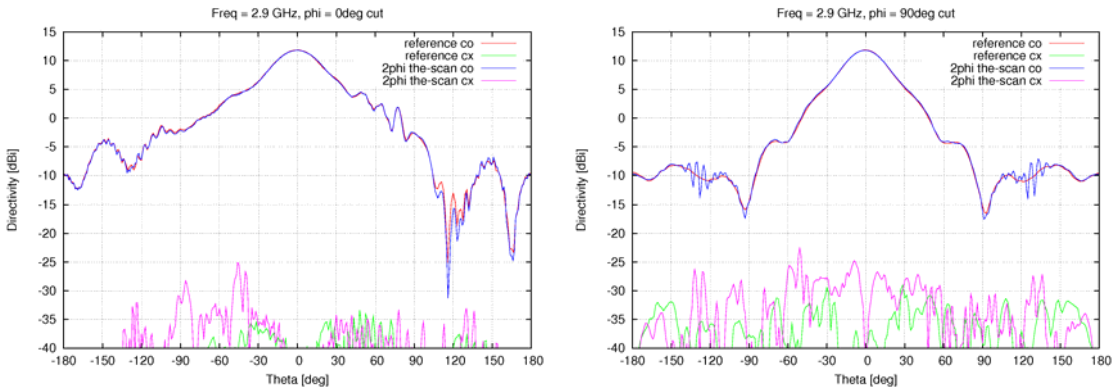

Fig. 18. Far-field pattern comparison from test 2 versus reference at 2.9 GHz (repeated test).

It can be seen from Figs. 17-18 that the cross-polar level noticeably reduced and the agreement for the cross-polar pattern became clearly better. The statistics for the difference between the co-polar pattern from tests 1 and test 2 and the reference pattern was calculated in the main beam region within $\theta = [0, \sim 10°]$. The standard deviation for the difference is shown in Table 5. It is seen that for the repeated tests the difference became smaller and does not exceed usual uncertainty of 0.05 dB (except for the test 2 at 1.5 GHz). It can also be noted that at the higher frequencies the difference was larger in the initial tests and noticeably smaller in the repeated tests as compared to the lower frequencies.

Table 5. Standard deviation for the difference between the co-polar pattern from tests 1 and test 2 and the reference pattern in the main beam region.

	Test 1				Test 2			
Freq. GHz	1.4	1.5	2.9	3.0	1.4	1.5	2.9	3.0
Initial	0.073	0.077	0.095	0.102	0.081	0.083	0.111	0.110
Repeated	0.052	0.052	0.036	0.030	0.052	0.063	0.026	0.036

Analyzing further the results in Figs. 17-18, it should be noted that the agreement in the cross-polar patterns is not quite perfect. This can partially be explained by the fact that the AUT may have changed from the initial to the repeated test and also by the fact that the 1-3 GHz probe calibration was not repeated with the 400 mm posts.

An interesting systematic deviation is seen in the results of test 2 in $\phi = 90°$ cut for $\theta \approx \pm 120°$ (Fig. 18, right). This strange pattern behavior was observed also in earlier tests of the double ϕ-step θ-scanning scheme, but it was explained by the properties of the laterally offset probe used in those tests. This time, the probe was very symmetric and the previous explanation could not be valid. An additional analysis was carried out and it was concluded that the observed pattern distortion most probably is caused by strong oscillations in the measured near-field signal, affected by the scattering from the antenna tower, and rearranged during the post-processing before the near-to-far-field transformation from the double ϕ-step θ-scanning scheme to the usual ϕ-scanning scheme.

6.4 Conclusions

The measured characteristics of the 1-3 GHz probe have shown that all requirements are clearly satisfied, with little compromise at the lower frequencies on relative pattern level in a narrow angular region. The probe represents a higher-order antenna when described in terms of spherical wave expansion and it must be used with the corresponding high-order probe correction technique.

The results of the tests where the 1-3 GHz probe was used for measurement of an electrically large AUT have shown that accurate AUT far-field pattern can be obtained with the main beam accuracy of the order of 0.05 dB (1σ).

An important observation was made when using the 1-3 GHz probe, in particular, with respect to its location on the probe tower. It is recommended to modify the probe support structure on top of the probe tower such that the probe can be placed in front of the absorbers.

Another observation was made regarding the scattering and shadow from the antenna tower and its possible effect on the results of the double ϕ-step θ-scanning scheme. It is recommended to carry out the test of the double ϕ-step θ-scanning scheme with another AUT, which is located close to the horizontal rotation axis.

7 0.4-1.2 GHz Probe: Manufacture and Validation

7.1 Manufacture of the 0.4-1.2 GHz probe

For the 0.4-1.2 GHz probe, the same electrical design as for the 1-3 GHz prototype probe, scaled by a factor of 2.5, was used. The 0.4-1.2 GHz probe thus has the dimensions $1\times1\times1.3$ m^3 and, if manufactured of solid aluminum, its estimated weight would be about 52 kg. In order to reduce the weight, an approach was considered in which some parts of the probe are made of aluminum and some parts are made of carbon fiber reinforced polymer (CFRP).

In order to ensure the high mechanical precision around the feed region, it was decided to manufacture the cavity and the bottom parts of the ridges from aluminum, while the major upper parts of the ridges to be made of CFRP and painted by conductive paint. The circular ground plane was decided to be made of 3 mm thick aluminum and it is sufficiently light. In addition, the thick walls of the cavity were made hollow to lighten it. The parts of the designed 0.4-1.2 GHz probe are shown in Fig. 19 with dark color marking the CFRP.

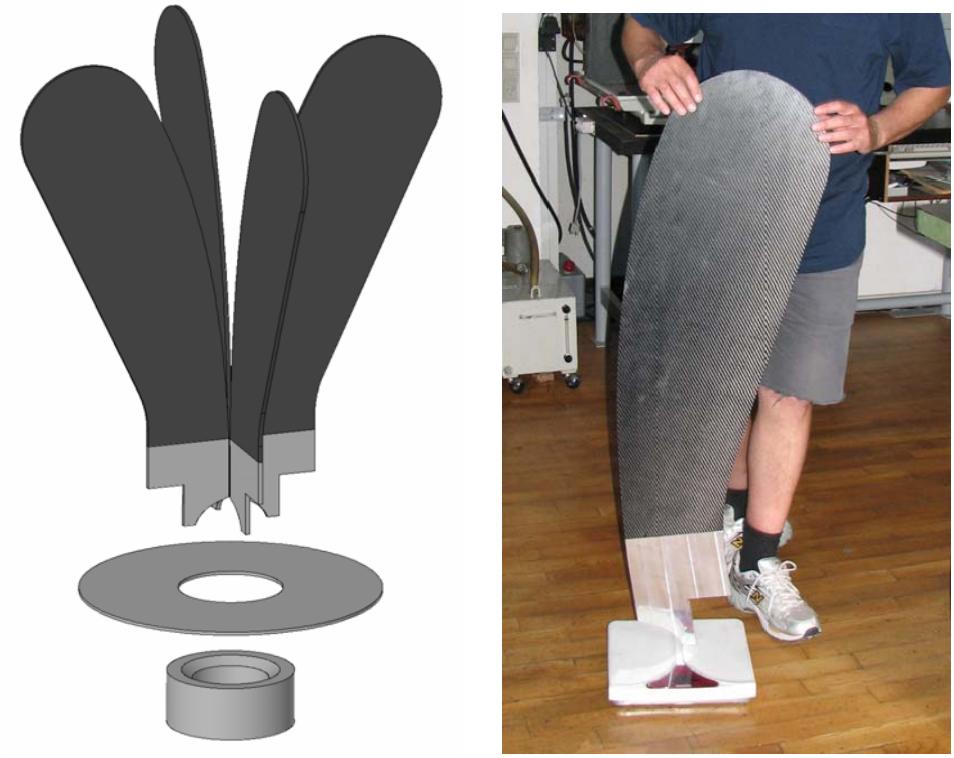

Fig. 19. Parts of the designed 0.4-1.2 GHz probe with dark color marking parts made of CFRP (left) and single assembled ridge being weighted (right).

The manufactured 0.4-1.2 GHz probe was delivered in the beginning of September 2011. The resulting weight of the manufactured hybrid Al-CFRP probe is 22.5 kg, which represents a reduction of weight by a factor of about 2.3 as compared to an entire aluminum antenna. The manufactured 0.4-1.2 GHz probe is shown in Fig. 20.

Fig. 20. Manufactured 0.4-1.2 GHz probe during pattern measurements.

7.2 S-parameters and radiation tests

Measurement of the S-parameters was carried out in anechoic environment with a calibrated HP8753D vector network analyzer in the frequency band 0.2-2.2 GHz at 401 points. The results are shown in Fig. 21 in the frequency band 0.2-2.0 GHz.

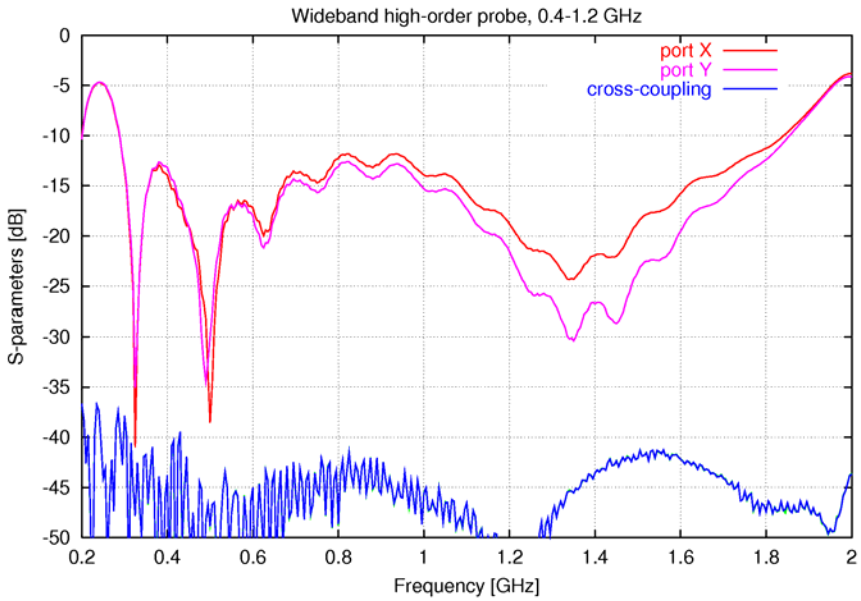

Fig. 21. Measured S-parameters of the 0.4-1.2 GHz probe.

It is seen from Fig. 21 that the S11 and S22 parameters are within the requirements in the band from 0.3-1.8 GHz, while the S21 and S12 parameters are well below the required –35 dB: generally, these are below –40 dB. Thus, the requirement on the S-parameters is completely satisfied.

The full-sphere radiation pattern of the 0.4-1.2 GHz probe was measured with the calibrated probe QRH615 in the band 0.35-1.80 GHz with the step of 0.05 GHz. The peak directivity is shown in Fig. 22, while the normalized radiation pattern at selected frequencies is shown in Fig. 23.

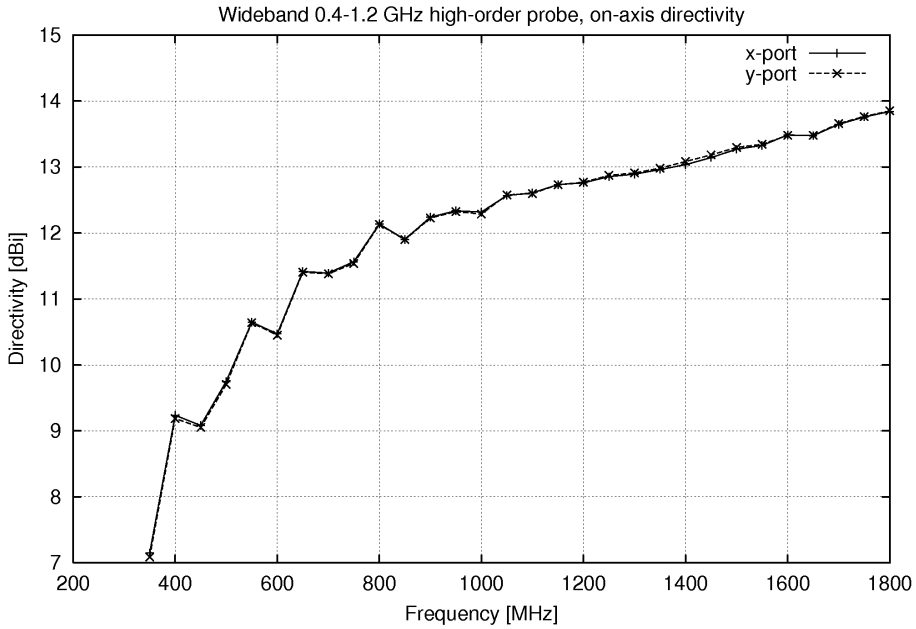

Fig. 22. Peak directivity of the 0.4-1.2 GHz probe.

The measured radiation pattern was analyzed for conformance to the requirements described in [AD8]. It was found that most of the pattern requirements are satisfied, in particular, requirement 2.1: pattern variation within $\theta = \pm 30°$ is < 10 dB at all frequencies, and requirement 2.3: front-to-back ratio is > 10 dB at all frequencies. The requirement 2.2: normalized pattern level within $\theta = \pm[50°…76°]$ to be < -10 dB is satisfied above 0.7 GHz, while between 0.5-0.7 GHz the maximum value of the normalized pattern level varies between –10…–8 dB with the highest value of –7.5 dB at 0.4 GHz. It is also noted that the observed behavior of the co-polar radiation pattern agrees very well with the simulation results.

The requirement 3: ports orthogonality, desirable polarization axial ratio > 35 dB, is completely satisfied at all frequencies within 0.4-1.2 GHz, the observed axial ratio values are typically larger than 45 dB.

The radiation efficiency is within 0…–0.45 dB through the frequency range 0.4-1.2 GHz; thus the requirement 6 is also satisfied.

It should be noted that at frequencies up to 1.8 GHz the main lobe becomes narrower, but the other parameters are within the requirements and thus the probe can be well used to measure antennas under test of slightly smaller size.

From the measured full-sphere radiation pattern, the spherical mode spectra were calculated (see Fig. 24) and analyzed. As expected, the 0.4-1.2 GHz probe clearly represents a higher-order probe with significant amount of power in the modes with $\mu \neq \pm 1$. It is also noted that noticeable level of the even μ-modes does not allow treating this probe as a pure odd-order probe.

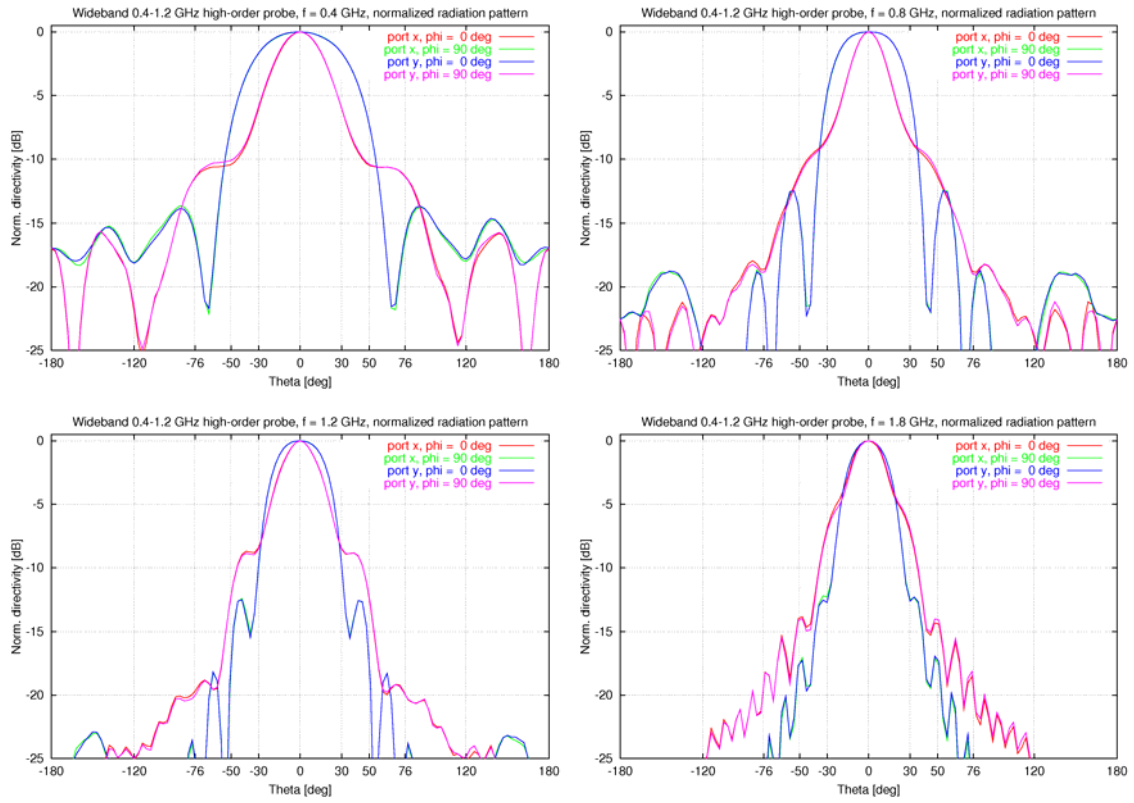

Fig. 23. Radiation pattern of the 0.4-1.2 GHz probe at selected frequencies.

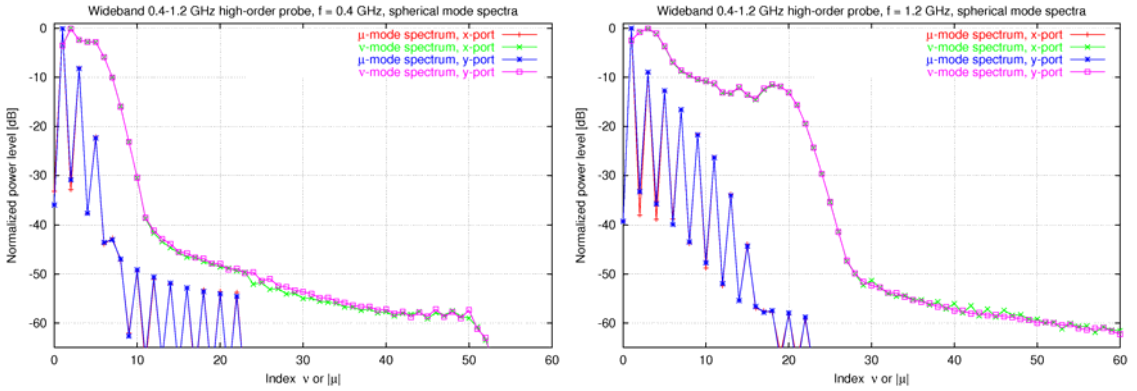

Fig. 24. Spherical mode spectra of the 0.4-1.2 GHz probe at 0.4 GHz and 1.2 GHz.

7.3 435 MHz first-order probe

Proper testing of the developed wideband 0.4-1.2 GHz probe and the corresponding antenna measurement procedure including higher-order probe correction requires comparison of an AUT test results obtained with the higher-order 0.4-1.2 GHz probe and with a first-order probe. This section outlines the design, manufacturing, and test results for the developed 435 MHz first-order probe.

The idea of light-weight first-order probes based on the electrically small antenna concept relies on the use of a spherical waveguide spatial filter instead of the cylindrical one [21]. It can be shown using the spherical wave theory that the sources confined to an electrically small volume radiate essentially the elementary dipole fields. On the

other hand, the directivity of a usual electrically small antenna is only 1.76 dBi, whereas the directivity of an optimum probe should be much higher. The problem can be overcome by arranging electrically small antenna elements in a superdirective array.

A first-order probe was designed as a superdirective array of magnetic dipoles on a circular ground plane, see Fig. 25. The probe is fed using a standard SMA connector from below the ground plane and it is matched to 50 Ohms around 431 MHz, see Fig. 25. This 4 MHz shift from the desired 435 MHz was investigated in details and it was found that it is due to anisotropy of the Rogers RO4003C substrate. After re-simulating the antenna assuming the substrate permittivity to be equal to the tangential permittivity component, an excellent agreement with the measurement results was obtained, see Fig. 25.

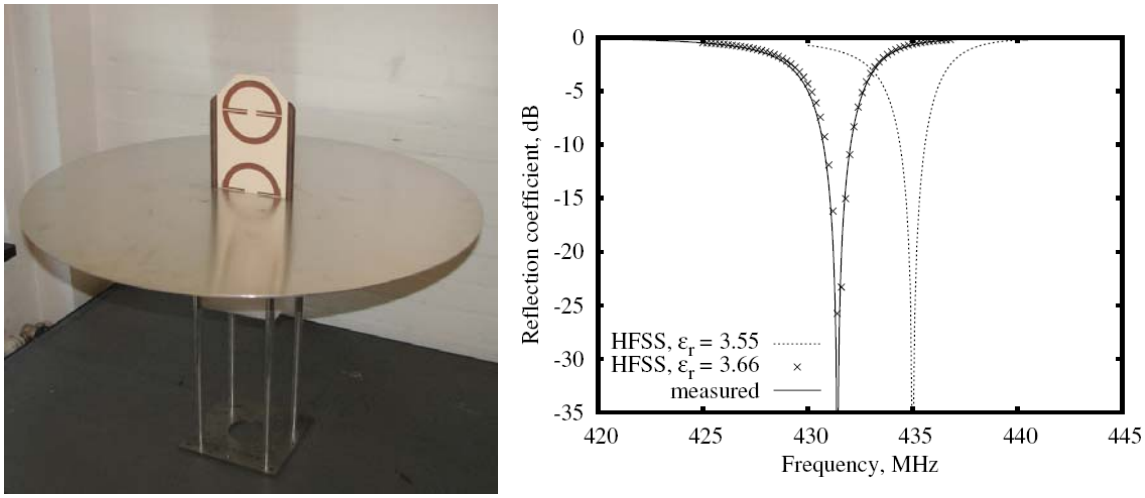

Fig. 25. Manufactured 435 MHz first-order probe and its measured and simulated reflection coefficient.

The radiation pattern of the first-order probe was measured at a series of frequencies around 430 MHz in order to investigate the frequency behavior of the spherical mode spectra. The measured radiation pattern at 431 MHz is shown in Fig. 26 for the case of feeding with the 180° hybrid. It is seen that the co-polar pattern is almost rotationally symmetric, i.e. E-plane and H-plane are almost equal, and the peak directivity is around 9 dBi.

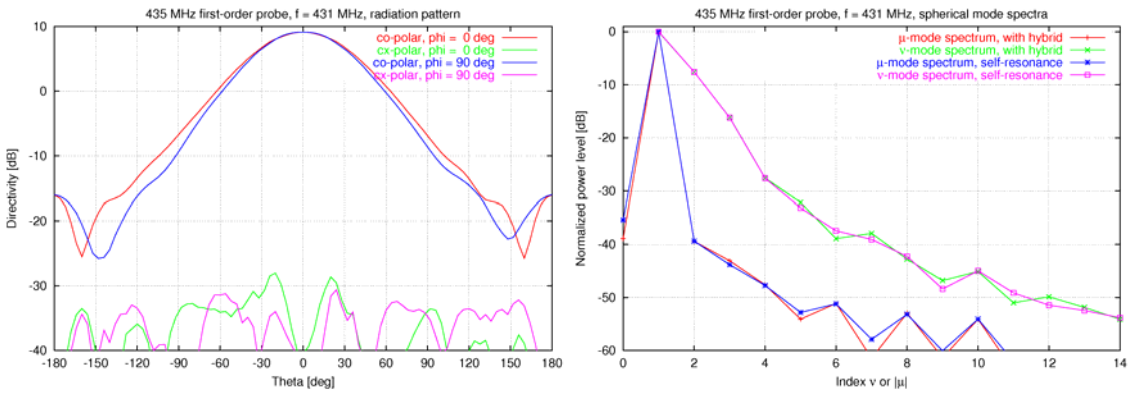

Fig. 26. Measured radiation pattern and spherical mode spectra of the first-order probe at 431 MHz.

From the measured radiation pattern, the spherical mode spectra were calculated and analyzed. It is seen from Fig. 26 that in a self-resonance regime the spectrum level for $\mu = 0$ is about –35 dB, while in the case of feeding with the 180° hybrid the spectrum level for $\mu = 0$ is around –39 dB. The spectrum level for the modes with $\mu > 1$ is below –39 dB. The first-order probe was fed with the 180° hybrid when it was used as a reference probe in the validation of antenna measurement procedure.

7.4 Verification of antenna measurement procedure

The detailed description of antenna measurement procedure verification with the 0.4-1.2 GHz probe is given in [AD14]. Only few representative results are included here.

Two antennas under test are defined to be an offset-mounted (AUT1) and a center-mounted (AUT2) SH400 horn. Since it was found in [AD12] that for an offset antenna the scattering and shadow from the antenna tower results in strong oscillations of the measured near-field signal, an additional, center-mounted AUT2 was introduced to investigate further the above effects. The AUT1 and AUT2 used in the measurements are shown in Fig. 27.

Fig. 27. Offset-mounted (AUT1) and center-mounted (AUT2) SH400 horn used as test object and the measurement coordinate system.

The reference measurements of the AUT1 and AUT2 were carried out at 1.1 GHz and 1.2 GHz with the 1-3 GHz probe and at 430 and 431 MHz with the first-order probe described in subsection 7.3.

Calibration of the 0.4-1.2 GHz high-order probe was carried out according to the updated measurement procedure; see section 4.1 and [AD7].

The measurement of the AUT1 was carried out using the ϕ-scanning scheme, while the measurement of the AUT2 was carried out two times: using the ϕ-scanning scheme and using the double-ϕ θ-scanning scheme.

The obtained AUT1 and AUT2 far-field patterns from measurements with the 0.4-1.2 GHz probe were then compared to the reference AUT1 and AUT2 far-field patterns. The plots with examples of pattern comparisons at 431 MHz and at 1.2 GHz are shown in Figs. 28-30. It is seen that both the co-polar and cross-polar patterns agree very well in all cases.

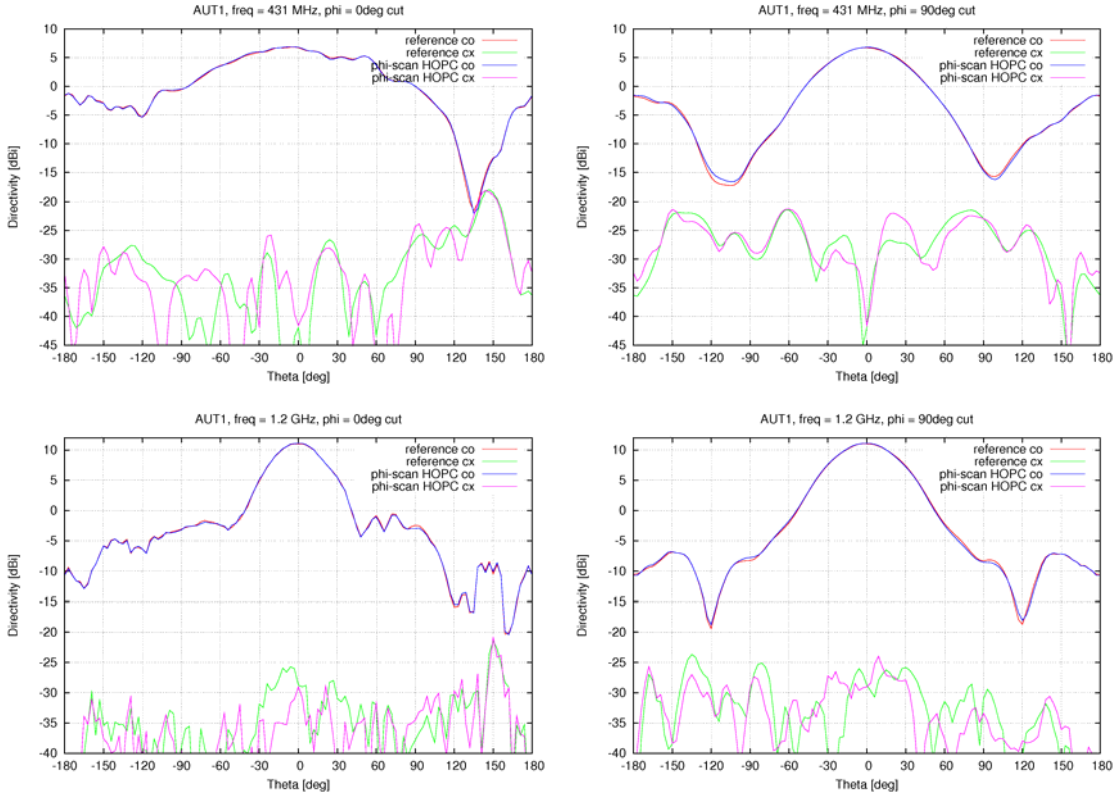

Fig. 28. Far-field pattern comparison for AUT1 at 431 MHz (top) at 1.2 GHz (bottom).

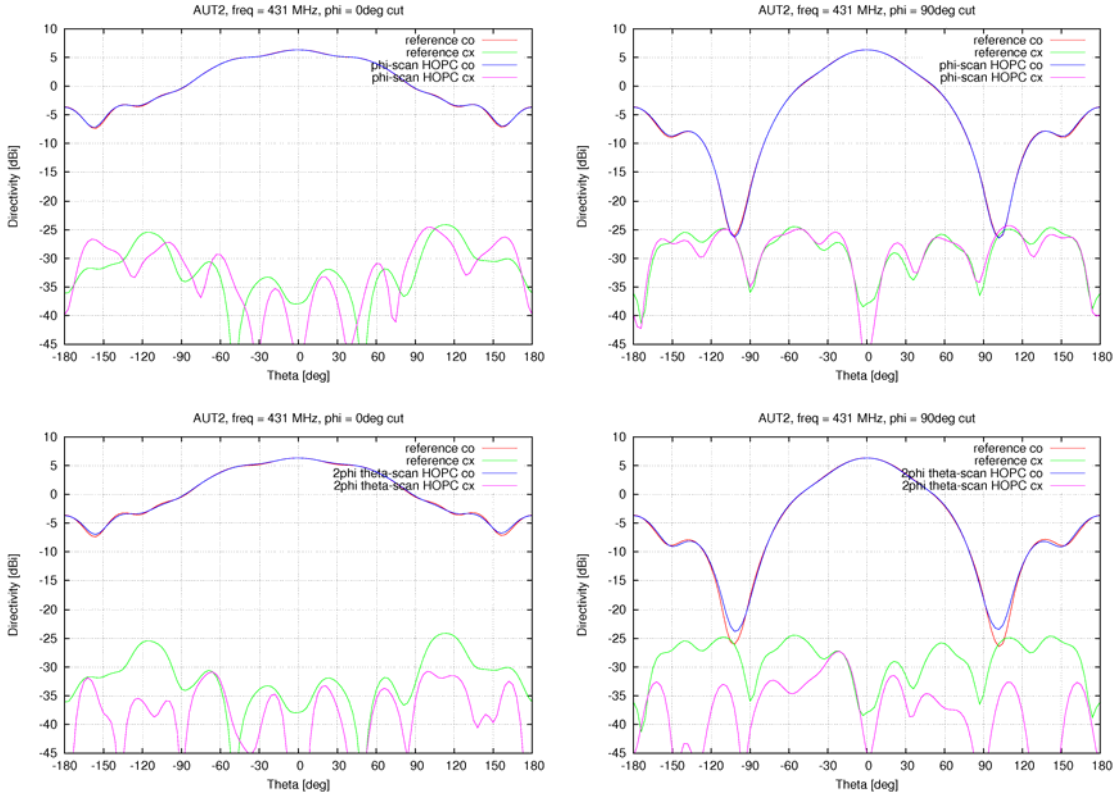

Fig. 29. Far-field pattern comparison for AUT2 at 431 MHz:
ϕ-scan (top) and 2ϕ θ-scan (bottom).

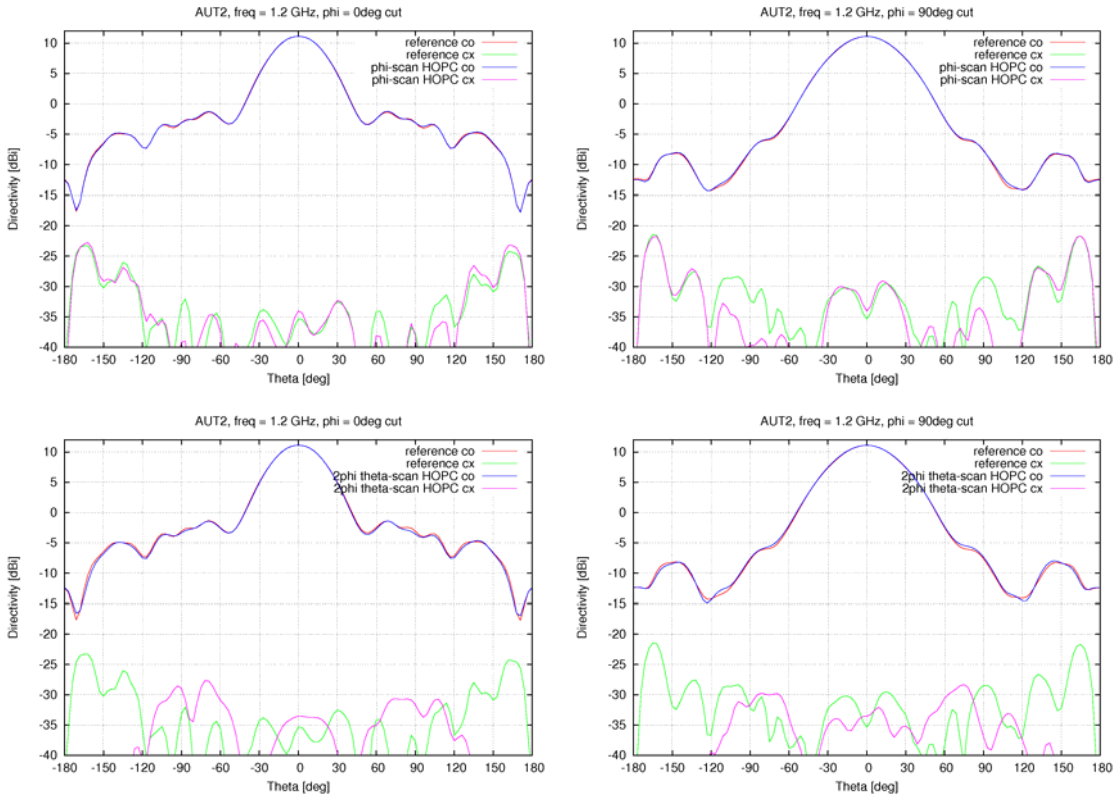

Fig. 30. Far-field pattern comparison for AUT2 at 1.2 GHz:
ϕ-scan (top) and 2ϕ θ-scan (bottom).

The statistics for the difference in dB between the co-polar patterns was calculated in the main beam region (3dB beamwidth) within θ = [0, 30°] at 430-431 MHz and within θ = [0, 20°] at 1.1-1.2 GHz. The standard deviation for the difference is shown in Table 6. It is seen that for the AUT1 the standard deviation is about 0.09 dB at 430-431 MHz, which might be caused by stronger influence of scattering and reflections for this challenging AUT at these low frequencies. At 1.1-1.2 GHz the standard deviation for the AUT1 decreases to some 0.06-0.07 dB. Assuming that the uncertainty of each result in this comparison is about the same, each of these uncertainties can be estimated as being about $\sqrt{2} = 1.4$ times smaller that the values in Table 6, thus in the worst case it does not exceed 0.06 dB (AUT1 at 430-431 MHz). For the AUT2 the standard deviation does not exceed 0.05 dB for all comparisons.

Table 6. Standard deviation for the difference in dB between the co-polar patterns in the main beam region.

Freq. MHz	AUT1 ϕ-scan	AUT2 ϕ-scan	AUT2 2ϕ θ-scan	AUT2 ϕ-scan vs. 2ϕ θ-scan
430	0.089	0.025	0.032	0.051
431	0.091	0.019	0.040	0.051
1100	0.069	0.042	0.039	0.008
1200	0.061	0.014	0.014	0.010

It was also observed that the cross-polar pattern obtained with the double-ϕ θ-scanning scheme has noticeably lower level for the data at 430-431 MHz, see Fig. 29. The

reference data in this case is the measurement with the 435 MHz first-order probe using the ϕ-scanning scheme.

For the data at 1.1-1.2 GHz, in Fig. 30, the cross-polar pattern obtained with the double-ϕ θ-scanning scheme has similar level, but different shape, as compared to the reference data, which is in this case the measurement with the 1-3 GHz higher-order probe using the ϕ-scanning scheme.

7.5 Conclusions

The measured characteristics of the 0.4-1.2 GHz probe have shown that all requirements are clearly satisfied, with little compromise at the lower frequencies on relative pattern level in a narrow angular region. The probe represents a higher-order antenna when described in terms of spherical wave expansion and it must be used with the corresponding higher-order probe correction technique.

The results of the tests where the 0.4-1.2 GHz probe was used for measurement of an electrically large AUT have shown that accurate AUT far-field pattern can be obtained. At frequencies around 430 MHz the main beam accuracy is estimated to be of the order of 0.06 dB (1σ) for a challenging offset-mounted AUT. For a center-mounted AUT the main beam accuracy is not worse than 0.03 dB (1σ). At frequencies around 1.2 GHz the main beam accuracy for an offset-mounted AUT does not exceed usual 0.05 dB (1σ), while for a center-mounted AUT the main beam accuracy is again not worse than 0.03 dB (1σ).

The measurement results obtained using the double-ϕ θ-scanning scheme have noticeable difference in the level and/or shape of the cross-polar patterns. More experience is necessary for this new scanning scheme applied to different types of antennas in order to understand its advantages and possible drawbacks.

8 Summary and Conclusions

In this project, the following was achieved:

A comparative investigation of higher-order probe correction techniques was carried out. The investigation was focused on the 3 entirely probe correction techniques that allow for general higher-order probes; these techniques are the FFT/matrix-inversion technique, the system matrix technique, and the plane wave near-field-far-field technique. The techniques were compared with respect to their scanning schemes, nominal computational complexities, and actual calculation times for some representative antennas and higher-order probes.

The FFT/matrix-inversion techniques was further developed by implementing the data processing for the double phi-step theta-scanning scheme, as well as in several computational aspects including a new computation scheme for the rotation coefficients, more efficient matrix pseudo-inverse implementation, and analysis and speed-up of the executable program. A normalization of the transmission formula was added, which improves on the condition numbers of the matrices to be solved and enables the use of an iterative solver, thus achieving a faster solution for the tested cases. Also, an outstanding issue with calculation of the channel balance has been clarified. The FFT/Matrix Inversion technique with double phi-step theta-scanning capability was extensively analyzed using both simulations and measurements.

The existing measurement procedure for first-order probe-corrected spherical near-field antenna measurements used at the DTU-ESA Facility was extended to accommodate the measurements with higher-order probes. The uncertainty budget was revisited to take into account the terms related to the use of higher-order probes.

A set of requirements to near-field probes for spherical near-field antenna measurements were specified. After a preliminary review of various antennas, the best candidate, an open-boundary quad-ridged horn, was selected. A thorough optimization was then performed to achieve a design meeting all the stringent requirements in the 1:3 frequency band.

Based on the proposed design, a 1-3 GHz probe prototype was manufactured at the mechanical workshop at the Department of Electrical Engineering at DTU. The measured characteristics of the 1-3 GHz probe have shown that all requirements are clearly satisfied, with little compromise at the lower frequencies on relative pattern level in a narrow angular region. The probe represents a higher-order antenna when described in terms of spherical wave expansion and it must be used with the corresponding high-order probe correction technique.

The results of the tests, where the 1-3 GHz probe was used for measurement of an electrically large AUT, have shown that accurate AUT far-field pattern is obtained with the main beam accuracy of the order of 0.05 dB (1σ).

The same electrical design, scaled by a factor of 2.5, was used for the 0.4-1.2 GHz probe. In order to reduce the weight of the probe, an approach was applied in which some parts of the probe are made of aluminum and some parts are made of carbon fiber reinforced polymer (CFRP). The manufactured 0.4-1.2 GHz probe has the weight of 22.5 kg, which represents a reduction by a factor of about 2.3 as compared to an entire aluminum antenna.

The measured characteristics of the 0.4-1.2 GHz probe have shown that all requirements are clearly satisfied. Accurate far-field pattern results were obtained from the tests where the 0.4-1.2 GHz probe was used for measurement of two representative AUTs. At frequencies around 430 MHz the main beam accuracy is estimated to be of the order of 0.06 dB (1σ) for a challenging offset-mounted AUT. For a center-mounted AUT the main beam accuracy is not worse than 0.03 dB (1σ). At frequencies around 1.2 GHz the main beam accuracy for an offset-mounted AUT does not exceed usual 0.05 dB (1σ), while for a center-mounted AUT the main beam accuracy is again not worse than 0.03 dB (1σ).

References

[1] T. Laitinen, S. Pivnenko, and O. Breinbjerg, "Iterative probe-correction technique for spherical near-field antenna measurements", *IEEE Antenna and Wireless Propagation Letters*, vol. 4, no. 1, pp. 221-223, 2005.

[2] T. Laitinen, S. Pivnenko, and O. Breinbjerg, "Application of the iterative probe-correction technique for a high-order probe in spherical near-field antenna measurements", *IEEE Antenna and Propagation Magazine*, vol. 48, no. 4, pp. 179-185, 2006.

[3] T. A. Laitinen, S. Pivnenko, and O. Breinbjerg," Odd-order probe correction technique for spherical near-field antenna measurements", *Radio Science*, vol. 40, no. 3, pp. 3009-3019, 2005.

[4] T.A. Laitinen, S. Pivnenko, "Probe correction technique for symmetric odd-order probes for spherical near-field antenna measurements", *IEEE Antennas and Wireless Propagation Letters*, 2007, pp. 635-638, 2007.

[5] T. Laitinen, O. Breinbjerg, "A first/third-order probe correction technique for spherical near-field antenna measurements using three probe orientations", *IEEE Transactions on Antennas and Propagation*, vol. 56, no. 5, pp. 1259-1268, May 2008.

[6] T. A. Laitinen, "Modified θ-scanning technique for first/third-order probes for spherical near-field antenna measurements," IEEE Transactions on Antennas and Propagation, vol. 57, no. 6, pp. 1590-1596, June 2009.

[7] T. Laitinen et al., "Development of 1-3GHz Probes for the DTU-ESA Spherical Near-Field Antenna Test Facility. Final Report, vol. 1: Executive Summary", Report R 729, Technical University of Denmark, December 2006.

[8] T. Laitinen, "Double phi-step theta-scanning technique for spherical near-field antenna measurements", *IEEE Transactions on Antennas and Propagation*, vol. 56, no. 6, pp. 1633-1639, June 2008.

[9] T. Laitinen et al. ,"Theory and practice of the FFT/matrix inversion technique for probe-corrected spherical near-field antenna measurements with high-order probes", *IEEE Trans. Antennas Propagat*., vol. 58, no. 8, pp. 2623-2631, August 2010.

[10] C.H. Schmidt, M.M. Leibfritz, T.F. Eibert, "Fully probe-corrected near-field far-field transformation employing plane wave expansion and diagonal translation operators", IEEE Transactions on Antennas and Propagation, vol. 56, no. 3, pp. 737-746, March 2008.

[11] C.H. Schmidt and T.F. Eibert, "Multilevel plane wave based near-field far-field transformation for electrically large antennas in free-space or above material halfspace", *IEEE Transactions on Antennas and Propagation*, vol. 57, no. 5, pp. 1382-1390, May 2009.

[12] T.B. Hansen, “Spherical near-field scanning with higher-order probes”, *IEEE Transactions on Antennas and Propagation*, vol. 59, no. 11, pp. 4049-4059, November 2011.

[13] T.B. Hansen, “Complex point sources in probe-corrected cylindrical near-field scanning”, *Wave Motion*, vol. 43, no. 8, pp. 700-712, 2006.

[14] T.B. Hansen, “Complex-point dipole formulation of probe-corrected cylindrical and spherical near-field scanning of electromagnetic fields”, *IEEE Transactions on Antennas and Propagation*, vol. 57, no. 3, pp. 728-741, March 2009.

[15] D.N. Black and E.B. Joy, "Test Zone Field Compensation", *IEEE Transactions on Antennas and Propagation*, vol. 43, no. 4, pp. 362-368, April 1995.

[16] J. T. Toivanen, T.A. Laitinen, S. Pivnenko, and L. Nyberg, ”Calibration of multi-probe antenna measurement system using test zone field compensation”, *European Conference on Antennas and Propagation – EuCAP 2009*, Berlin, March 2009.

[17] R. Pogorzelski, “Extended probe instrument calibration (EPIC) for accurate spherical near-field antenna measurements”, *IEEE Transactions on Antennas and Propagation*, vol. 57, no. 10, pp. 3366-3371, October 2009.

[18] R. Pogorzelski, “Experimental demonstration of the extended probe instrument calibration technique”, *IEEE Transactions on Antennas and Propagation*, vol. 58, no. 6, pp. 2093-2097, June 2010.

[19] S. Pivnenko, J. M. Nielsen, O. Breinbjerg, T. Laitinen, T.B. Hansen “Comparison of the FFT/matrix inversion and system matrix techniques for higher-order probe correction in spherical near-field antenna measurements”, 33’rd ESA Antenna Workshop, Noordwijk, The Netherlands, October 2011

[20] J. E. Hansen (Ed.), *Spherical Near-Field Antenna Measurements*. London, UK: Peter Peregrinus Ltd., 1988.

[21] O.S. Kim, S. Pivnenko, and O. Breinbjerg: Superdirective Magnetic Dipole Array as a First-Order Probe for Spherical Near-Field Antenna Measurements, to appear in *IEEE Transactions on Antennas and Propagation*, vol. 60, no. 10, 2012.